Defence Technology 16 (2020) 1019–1038

Contents lists available at ScienceDirect

Defence Technology

journal homepage: www.keaipublishing.com/en/journals/defence-technology

Influence of active constrained layer damping on the coupled vibration response of functionally graded magneto-electro-elastic plates with skewed edges

M. Vinyas [a], D. Harursampath [a], T. Nguyen-Thoi [b, c, *]

[a] Nonlinear Multifunctional Composites Analysis and Design (NMCAD) Laboratory, Department of Aerospace Engineering, Indian Institute of Science, Bangalore, 560012, India
[b] Division of Computational Mathematics and Engineering, Institute for Computational Science, Ton Duc Thang University, Ho Chi Minh City, Viet Nam
[c] Faculty of Civil Engineering, Ton Duc Thang University, Ho Chi Minh City, Viet Nam

ARTICLE INFO

Article history:
Received 30 September 2019
Received in revised form
10 November 2019
Accepted 28 November 2019
Available online 4 December 2019

Keywords:
Vibration control
Functionally graded
MEE plates
Skew angle
Active constrained layer damping (ACLD) patches

ABSTRACT

This article makes the first attempt in assessing the influence of active constrained layer damping (ACLD) treatment towards precise control of frequency responses of functionally graded skew-magneto-electro-elastic (FGSMEE) plates by employing finite element methods. The materials are functionally graded across the thickness of the plate in terms of modest power-law distributions. The principal equations of motion of FGSMEE are derived via Hamilton's principle and solved using condensation technique. The effect of ACLD patches are modelled by following the complex modulus approach (CMA). Additionally, distinctive emphasis is laid to evaluate the influence of geometrical skewness on the attenuation capabilities of the plate. The accuracy of the current analysis is corroborated with comparison of previous researches of similar kind. Additionally, a complete parametric study is directed to understand the combined impacts of various factors like coupling fields, patch location, fiber orientation of piezoelectric patch in association with skew angle and power-law index.

1. Introduction

A novel class of composite materials known as functionally graded materials (FGMs) emerged to fulfil the high demands of improved structural performance requirements. The effective properties or functional performance of these materials exhibit variation in one or more spatial direction. In other words, the material properties of FGMs are non-homogeneous and are position dependent. Hence, such materials are designed to provide predictable properties by virtue of their discrete constituents. In contrast to the conventional materials, FGMs display a better ability to control deformation, dynamic response, multifunctionality etc. which are beneficial to vibration control of the structures. Due to these advantageous properties, FGMs are the potential candidates for various complex engineering applications such as military, automotive, biomedical application, semiconductor industry, manufacturing industry and general structural elements in thermal environments.

Magneto-electro-elastic (MEE) composites are the combination of piezoelectric (PE) and piezomagnetic (PM) phases, where in a triple energy conversion among magnetic, electric and elastic fields can be observed. Further, MEE materials display high degree of magneto-electric coupling which cannot be seen in individual phases. Therefore, it is very crucial to assess the associated electromagnetism phenomenon either experimentally or with the aid of sophisticated computational techniques [1,2]. The topological textures and concentration of Barium Titanate and Cobalt Ferrite have a direct impact on the operative material properties associated with the degree of coupling exhibited by the MEE entities [3,4]. This advantage can be used extensively for the creation of various devices where couplings among the said phases are needed. Also, through the sensitivity analysis [5] the performance optimization can also be achieved effectively. The functionally

* Corresponding author. Division of Computational Mathematics and Engineering, Institute for Computational Science, Ton Duc Thang University, Ho Chi Minh City, Viet Nam.
E-mail addresses: vinyasmahesh@iisc.ac.in (M. Vinyas), dinesh@aero.iisc.ernet.in (D. Harursampath), nguyenthoitrung@tdtu.edu.vn (T. Nguyen-Thoi).
Peer review under responsibility of China Ordnance Society

https://doi.org/10.1016/j.dt.2019.11.016

graded magneto-electro-elastic (FGMEE) materials can further intensify the desirable characteristics of their individual phases. For instance, the MEE structures exhibit high electric properties on the piezoelectric side while the magnetic behavior is taken care by the piezomagnetic phase.

To this end, many pioneers have devoted themselves to evaluating the mechanical responses of homogeneous as well as functionally graded MEE structures. Among them, a significant contribution was made by Pan and his associates in developing the exact solutions to facilitate the natural vibrational analysis of multilayered MEE plates [6,7]. Lage et al. [8] implemented partial mixed layer-wise finite element (FE) methods and explored the frequency response of MEE plates. Moita et al. [9] assessed the vibrational features of MEE plates utilizing the higher-order shear deformation theory. Meanwhile, a variety of computational practices have proven to be effective in the evaluation of the static and natural vibration characteristics of MEE plates. These include, the approximate solution method [10], finite elements methods [11–18], mesh-less method [19] and state-space approach [20–24] among others. Furthermore, numerous layer-wise models also aid the accurate analysis of MEE structures [25–29]. Also, the machine learning techniques can also prove to be effective in assessing the vibration control and energy harvesting of coupled MEE structures in the near future [30,31].

Emphasizing more on the compositionally graded MEE materials, Pan and Han [32] presented an exact solution for the FGMEE rectangular plate. Also, Huang et al. [33] presented methodical solutions to assess the behavior of FGMEE plane beams. Bhangale and Ganesan [34] investigated the vibrational behavior of FGMEE plates using finite elements method. Wu and Tsai [35] probed the static response of doubly curved FGMEE shells subjected to various forms of loading through an asymptotic approach. Li et al. [36] considered the influence of uniform load on FGMEE circular plate in their work. Sladek et al. [37] evaluated the bending response of FGMEE circular plate by employing a meshless method. Meanwhile, Kiran et al. [38] assessed the free vibrations and static behavior of porous MEE plates. Stepped functionally graded MEE structures were built and their static behavior was studied for varying compositions of Barium Titanate and Cobalt Ferrite [39–43].

It is well known that the hazardous vibrations experienced by a structure may have an adverse effect on the performance and service period. These undesirable oscillations can be effectually dampened by embedding a monolithic piezoelectric patch provided with an external voltage to the host structure. The piezoelectric patch performs the function of a sensor or an actuator or both [44]. This combined arrangement to negate the vibrations is designated as active constrained layer damping (ACLD) treatment. Nonetheless, greater attenuation capabilities are witnessed in patches composed of epoxy matrices with inclusions of piezoelectric fibers (1–3 PZC) when compared to the monolithic piezoelectric patch [45]. In addition to this functionality, the 1–3 PZC requires a lower control voltage. The ACLD treatment is comprised of the 1–3 PZC patch in combination with a visco-elastic layer. The former serves as the constraining layer with the latter, as the constrained layer. Therefore, it is obligatory that the viscoelastic layer dispels high energy through enhanced shear deformations.

Various studies have upheld the cause of ACLD treatments in the vibrational damping of the structures. Controlling the frequency response of composite plates through incorporation of vertically reinforced 1–3 PZC patch were validated by Ref. [46]. They also suggested a model to gauge the impact of the ACLD usage on FGMs [47–49], laminated [50–52] and sandwiched plates [53,54]. Their study proved that ACLD treatments can provide remarkable attenuations of linear and non-linear vibration of structures. The frequency behavior of composite plates and doubly-curved shells subjected to ACLD treatment were impacted by geometric skew as mentioned by Kanasogi and Ray [55]. Kattimani and Ray [56] adopted this unique technique to MEE structures. They carried out similar investigations on FG and multiferroic magneto-electro-elastic plates [57,58]. Whereas, Vinyas [59,60] proposed an FE based method to probe the regulated linear frequency behavior of skewed MEE plates consisting of multiple layers.

Very minimal works have been carried out to gauge the impact of ACLD treatments on functionally-graded skew magneto-electro-elastic (FGSMEE) plates. To the best of the author's awareness, the current work is the first of its kind in evaluating the damped frequency response of FGSMEE plates subjected to the ACLD treatment. This makes the requirement of the present study to be an inevitable one. Therefore, an FE formulation is presented with the assistance of the Hamilton's principle. The damping abilities of ACLD treated FGSMEE plates are thoroughly investigated to assess the major influences of geometric parameters like skew angles, patch positions and material parameters such as power-law index and coupling fields.

2. Problem statement

In this study, the controlled response of functionally graded skew magneto-electro-elastic (FGSMEE) plate has been evaluated. To this end, the ACLD treated FGSMEE plate with length a, width b, and thickness H is considered along x-, y- and z-axes of Cartesian coordinates, respectively and illustrated in Fig. 1. h_v and h_p correspond to the thickness of the visco-elastic and 1–3 PZC layers, respectively. The skewed edge of the FGSMEE plate and the angle of alignment of the piezoelectric fibres of the 1–3 PZC patch are given

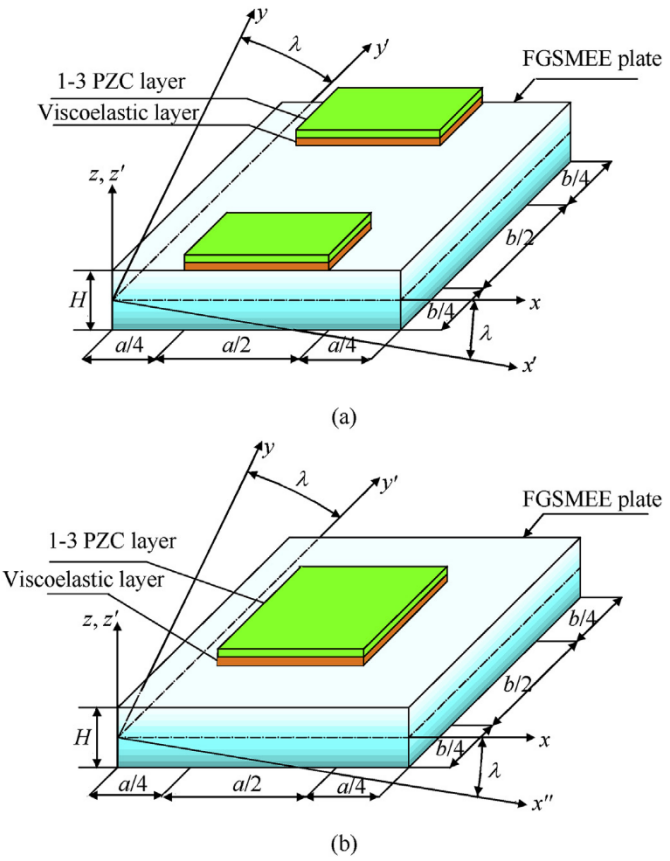

Fig. 1. FGSMEE plate with (a) edge ACLD patch (b) centre ACLD patch.

by λ and α, respectively.

2.1. Material properties and methods

The present research considers functionally graded magneto-electro-elastic materials (FGMEEM). The coupled constitutive equations of FGMEEM as a function of z-coordinate can be represented as follows [57]:

$$\begin{aligned}
\left\{\sigma_b^{fg}(z)\right\} &= \left[\overline{C}_b^{fg}(z)\right]\left\{\varepsilon_b^{fg}\right\} - \left\{\overline{e}_b^{fg}(z)\right\}E_z - \left\{\overline{q}_b^{fg}(z)\right\}H_z \\
\left\{\sigma_s^{fg}(z)\right\} &= \left[\overline{C}_s^{fg}(z)\right]\left\{\varepsilon_s^{fg}\right\} \\
D_z(z) &= \left\{\overline{e}_b^{fg}(z)\right\}^{\mathrm{T}}\left\{\varepsilon_b^{fg}\right\} + \overline{\in}_{33}^{fg}(z)E_z + \overline{d}_{33}^{fg}(z)H_z \\
B_z(z) &= \left\{\overline{q}_b^{fg}(z)\right\}^{\mathrm{T}}\left\{\varepsilon_b^{fg}\right\} + \overline{d}_{33}^{fg}(z)E_z + \overline{\mu}_{33}^{fg}(z)H_z
\end{aligned} \tag{1}$$

in which, superscript fg signifies that the material is functionally graded. The material properties $[\overline{C}_b^{fg}(z)]$ and $[\overline{C}_s^{fg}(z)]$ represent the elastic coefficient matrix. $\{\overline{q}_b^{fg}(z)\}$, $\{\overline{e}_b^{fg}(z)\}$ correspond to the magnetostrictive co-efficient matrix and piezoelectric co-efficient matrix, respectively. $\overline{\in}_{33}^{fg}(z)$ and $\overline{d}_{33}^{fg}(z)$, are the dielectric and electromagnetic coefficients, respectively. The perpendicular electric displacement and the magnetic induction components are D_z and B_z, respectively. E_z and H_z are the transverse electrical and magnetic field components, respectively. The various coefficient matrices appearing in Eq. (1) are illustrated in Appendix-A.

A simple-power law distribution is assumed to depict the variation of the effective material properties along the thickness of FGSMEE plate, as a function of volume fraction and constituent material properties. Further, the variation of the volume fraction is governed by the power-law index 'r'. Two forms of FG material property distribution are considered for evaluation. One being, Barium Titanate rich Bottom (B-rich) and the other Cobalt Ferrite rich Bottom (F-rich). The notation B-rich bottom suggests that the bottom layer of the FGSMEE plate is purely piezoelectric (PE) which smoothly and continuously varies to the pure piezomagnetic (PM) phase at the top layer. Analogously, the vice-versa of this arrangement holds good for 'F rich Bottom'. Encapsulating all these, the effective material properties of the FGSMEE plate can be illustrated as follows [57]:

$$\begin{aligned}
&\left[\overline{C}_b^{fg}(z)\right] = [\overline{C}_b]_F + ([\overline{C}_b]_B - [\overline{C}_b]_F)V_{fg};\ \left[\overline{C}_s^{fg}(z)\right] = [\overline{C}_s]_F + ([\overline{C}_s]_B - [\overline{C}_s]_F)V_{fg}; \\
&\left[\overline{q}^{fg}(z)\right] = [\overline{q}]_F + ([\overline{q}]_B - [\overline{q}]_F)V_{fg};\ \left[\overline{e}^{fg}(z)\right] = [\overline{e}]_F + ([\overline{e}]_B - [\overline{e}]_F)V_{fg}; \\
&\left[\overline{\mu}^{fg}(z)\right] = [\overline{\mu}]_F + ([\overline{\mu}]_B - [\overline{\mu}]_F)V_{fg};\ \left[\overline{\in}^{fg}(z)\right] = [\overline{\in}]_F + ([\overline{\in}]_B - [\overline{\in}]_F)V_{fg}; \\
&\left[\overline{d}^{fg}(z)\right] = [\overline{d}]_F + ([\overline{d}]_B - [\overline{d}]_F)V_{fg};
\end{aligned} \tag{2}$$

where, the subscripts B and F denote pure PE and PM phases, respectively. Also, V_{fg} is the volume fraction of the functionally graded layer which can be given by,

$$\begin{aligned}
V_{fg} &= \left(\frac{z-h_2}{h_1-h_2}\right)^r, \text{ for B-rich bottom and F-rich top} \\
V_{fg} &= \left(\frac{z-h_1}{h_2-h_1}\right)^r, \text{ for F} - \text{rich bottom and B} - \text{rich top}
\end{aligned} \tag{3}$$

here, r is the power-law index.

Further, h_1 and h_2 are the z-coordinate of the bottom and top surfaces of FGSMEE plate, respectively. The material properties of 1–3 PZC, pure PM and pure PE phases are mentioned in Table 1.

Meanwhile, the constitutive equations of the 1–3 PZC layer of the ACLD patch can be mentioned as follows [57]:

$$\begin{aligned}
\left\{\sigma_b^P\right\} &= \left[\overline{C}_b^P\right]\left\{\varepsilon_b^P\right\} - \left[\overline{C}_{bs}^P\right]\left\{\varepsilon_s^P\right\} - \left\{\overline{e}_b^P\right\}E_z \\
\left\{\sigma_s^P\right\} &= \left[\overline{C}_{bs}^P\right]^{\mathrm{T}}\left\{\varepsilon_b^P\right\} + \left[\overline{C}_s^P\right]\left\{\varepsilon_s^P\right\} - \left\{\overline{e}_b^P\right\}E_z \\
D_z^P &= \left\{\overline{e}_b^p\right\}^{\mathrm{T}}\left\{\varepsilon_b^P\right\} + \left\{\overline{e}_s^p\right\}^{\mathrm{T}}\left\{\varepsilon_s^P\right\} + \overline{\in}_{33}^P E_z^P
\end{aligned} \tag{4}$$

The material property matrices of Eq. (4) are illustrated in Appendix-A (Eqs. (A-2) and (A-3)).

The visco-elastic layer of the ACLD patch is modelled via complex modulus approach (CMA) [61]:

$$G = G^{'}(1+i\eta);\ E = 2G(1+\nu) \tag{5}$$

where, $G^{'}$, η and ν are the storage modulus, loss factor and Poisson's ratio of the viscoelastic layer, respectively.

As the elastic waves propagate several magnitudes slower than electro-magnetic waves, a quasi-static approximation of electro-magnetic fields can be considered [28,29]. Hence, the distribution of E_z and B_z through the FGSMEE plate is linked to the electric (φ) and magnetic scalar potentials (ψ) according to the Maxwell's electromagnetic equations as given below

$$E_z = -\frac{\partial\varphi}{\partial z}H_z = -\frac{\partial\psi}{\partial z} \tag{6}$$

The variation of φ and ψ across the thickness is assumed to be linear as the thickness of the plate is small. It can be illustrated as follows:

$$\varphi = \frac{z-h_1}{H}\overline{\varphi};\ \psi = \frac{z-h_1}{H}\overline{\psi} \tag{7}$$

where, $\overline{\varphi}$ and $\overline{\psi}$ are the electric and magnetic potential at the top surface of FGSMEE plate, respectively.

2.2. Kinematics of FGSMEE plate deformations

The Layerwise shear deformation model used to govern the kinematic deformations can be represented as follows [59]:

$$\begin{aligned}
u &= u_0 + \left(z - \langle z - \frac{h}{2}\rangle\right)\theta_x + \left(\langle z - \frac{h}{2}\rangle - \langle z - h_{N+2}\rangle\right)\kappa_x + \langle z - h_{N+2}\rangle\gamma_x \\
v &= v_0 + \left(z - \langle z - \frac{h}{2}\rangle\right)\theta_y + \left(\langle z - \frac{h}{2}\rangle - \langle z - h_{N+2}\rangle\right)\kappa_y + \langle z - h_{N+2}\rangle\gamma_y
\end{aligned} \tag{8}$$

in which, u and v are the axial displacements along x- and y-, respectively. Meanwhile, the terms u_0 and v_0 represent the translational displacements of any point lying on the mid-surface along x- and y-axes, respectively. The generalized rotations of the normal to mid-plane of the substrate, viscoelastic layer and piezoelectric patch about the y-axis are denoted by θ_x, κ_x and γ_x, respectively. Similarly θ_y, κ_y and γ_y represents the same about the x-axis. The displacement continuity condition between the adjacent continua can be satisfied with the help of the singularity function denoted within the brackets.

To accomplish effective vertical actuation of ACLD treatment and to enhance the accuracy of the results, a higher order transverse displacement model is assumed in the present analysis, which was neglected in Kanasogi and Ray [55].

Table 1
Material properties corresponding to $BaTiO_3 - CoFe_2O_4$ and 1–3 PZC patch ([55,59]).

Material property	Material constants	Piezomagnetic (F)	Piezoelectric (B)	1-3 PZC
Elastic constants	$C_{11} = C_{22}$	286	166	9.29
/GPa	C_{12}	173	77	6.18
	$C_{13} = C_{23}$	170	78	6.05
	C_{33}	269.5	162	35.44
	$C_{44} = C_{55}$	45.3	43	1.58
	C_{66}	56.5	44.5	1.54
Piezoelectric constants	$e_{31=}\, e_{32}$	0	−4.4	−0.1902
/(C·m^{-2})	e_{33}	0	18.6	18.4107
	$e_{15=}\, e_{24}$	0	11.6	0.004
Dielectric constant	$\varepsilon_{11} = \varepsilon_{22}$	0.08	11.2	–
/(10^{-9} C^2·Nm^{-2})	ε_{33}	0.093	12.6	–
Magnetic permeability	$\mu_{11} = \mu_{22}$	5.9	0.05	–
/(10^{-4} N^2· C^{-2})	μ_{33}	1.57	0.1	–
Piezomagnetic constants	$q_{31} = q_{32}$	580	0	–
/(N·Am^{-1})	q_{33}	700	0	–
	$q_{15} = q_{24}$	560	0	
Density/(kg·m^{-3})	ρ	5300	5800	5090

$$w = w_0 + z\theta_z + z^2\kappa_z \tag{9}$$

where, w_0 refers to the transverse displacement at any point on the reference plane,θ_z and κ_z are the generalized displacements representing the gradients of the transverse displacement in the FGSMEE substrate plate and the viscoelastic layer, respectively with respect to thickness coordinate.

The generalized displacement components are categorized as follows:

$$\{d_t\} = [u_0 \quad v_0 \quad w_0]^{\mathrm{T}}; \{d_r\} = [\theta_x \quad \theta_y \quad \theta_z \quad \kappa_z \quad \kappa_x \quad \kappa_y \quad \gamma_x \quad \gamma_y]^{\mathrm{T}} \tag{10}$$

The strain vectors can be classified as the shear strain vector $\{\varepsilon_s\}$ comprising of transverse shear strains and the bending strain vector $\{\varepsilon_b\}$ constituting of in-plane shear strain and normal strains, which can be illustrated as follows:

$$\{\varepsilon_b\} = \{\varepsilon_x \quad \varepsilon_y \quad \varepsilon_z \quad \varepsilon_{xy}\}^{\mathrm{T}}; \{\varepsilon_s\} = \{\varepsilon_{xz} \quad \varepsilon_{yz}\}^{\mathrm{T}} \tag{11}$$

where, ε_x, ε_y and ε_z are the normal strains along *x*-, *y*-and *z*-axes, respectively. Further, ε_{xy} is the in-plane shear strain; ε_{xz} and ε_{yz} are the transverse shear strains. The strain vector $\{\varepsilon_b\}$ corresponding to any point lying in FGSMEE plate and 1–3 PZC layer, respectively can be shown as follows:

$$\begin{Bmatrix} \varepsilon_b^{fg} \end{Bmatrix} = \{\varepsilon_{bt}\} + [Z_1]\{\varepsilon_{rb}\}$$
$$\begin{Bmatrix} \varepsilon_b^{P} \end{Bmatrix} = \{\varepsilon_{bt}\} + [Z_2]\{\varepsilon_{rb}\} \tag{12}$$

Similarly, transverse shear strain vectors $\{\varepsilon_s\}$ associated with the different layers of ACLD treated FGSMEE plate can be depicted as follows:

$$\begin{Bmatrix} \varepsilon_s^{fg} \end{Bmatrix} = \{\varepsilon_{ts}\} + [Z_3]\{\varepsilon_{rs}\}$$
$$\begin{Bmatrix} \varepsilon_s^{Vis} \end{Bmatrix} = \{\varepsilon_{ts}\} + [Z_4]\{\varepsilon_{rs}\} \tag{13}$$
$$\begin{Bmatrix} \varepsilon_s^{P} \end{Bmatrix} = \{\varepsilon_{ts}\} + [Z_5]\{\varepsilon_{rs}\}$$

where, the superscripts *P* and *V* is correspond to the 1–3 PZC layer and viscoelastic layers of ACLD patch, respectively. The different strain-displacement sub matrices along with the various transformation matrices $[Z_1]$ to $[Z_5]$ mentioned in Eqs. (12) and (13) are shown in Appendix (Eq. (B-2)).

2.3. Finite element formulation

In order to model the geometry of FGSMEE plates, an eight noded isoparametric quadrilateral element is used. The generalized degrees of freedom can be represented as follows:

$$\{d_{ti}\} = [u_{0i} \quad v_{0i} \quad w_{0i}]^{\mathrm{T}}; \{d_{ri}\} = [\theta_{xi} \quad \theta_{yi} \quad \theta_{zi} \quad \kappa_{zi} \quad \kappa_{xi} \quad \kappa_{yi} \quad \gamma_{xi} \quad \gamma_{yi}]^{\mathrm{T}} \quad (i = 1, 2 \ldots 8) \tag{14}$$

Further, using displacement approximations, the generalized displacement vectors$\{d_t\}$ and $\{d_r\}$, electric potential φ and magnetic potential ψ at any point within the element can be represented in terms of the nodal displacement vectors $\{d_t^e\}$ and $\{d_r^e\}$, nodal electric potential $\{\varphi^e\}$ and nodal magnetic potential $\{\psi^e\}$, respectively, as follows:

$$\{d_t\} = [N_t]\{d_t^e\}; \{d_r\} = [N_r]\{d_r^e\}; \varphi = [N_\varphi]\{\varphi^e\}; \psi = [N_\psi]\{\psi^e\} \tag{15}$$

where,

$$\{d_t^e\}=\left[\{d_{t1}\}^{\mathbf{T}}\{d_{t2}\}^{\mathbf{T}}\ldots\{d_{t8}\}^{\mathbf{T}}\right]^{\mathrm{T}};\{d_r^e\}=\left[\{d_{r1}\}^{\mathbf{T}}\{d_{r2}\}^{\mathbf{T}}\ldots\{d_{r8}\}^{\mathbf{T}}\right]^{\mathrm{T}}$$
$$[N_t]=[N_{t1}N_{t2}\ldots N_{t8}],N_{ti}=N_iI_t,[N_r]=[N_{r1}N_{r2}\ldots N_{r8}],N_{ri}=N_iI_r$$
$$\{\varphi^e\}=[\varphi_1\ \varphi_2\cdots\varphi_8]^{\mathrm{T}};\{\psi^e\}=[\psi_1\ \psi_2\cdots\psi_8]^{\mathrm{T}};$$
$$[N_\psi]=[N_\varphi]=[N_1\,N_2\ldots N_8] \tag{16}$$

in which, N_i is the natural coordinate shape function associated with the ith node of the eight noded isoparametric quadrilateral element used. $[N_t]$, $[N_r]$, $[N_\varphi]$ and $[N_\psi]$ are the shape function matrices. I_t and I_r are identity matrices.

The electric and magnetic fields depicted in Eq. (6) can hence be expressed as follows:

$$E_z=-\frac{1}{H}[N_\varphi]\{\varphi^e\};H_z=-\frac{1}{H}[N_\psi]\{\overline{\psi}^e\} \tag{17}$$

Considering the above FE quantities, the strain-displacement relationship can be established by

$$\{\varepsilon_{bt}\}=[B_{tb}]\{d_t^e\},\{\varepsilon_{rb}\}=[B_{rb}]\{d_r^e\},\{\varepsilon_{ts}\}=[B_{ts}]\{d_t^e\},\{\varepsilon_{rs}\}=[B_{rs}]\{d_r^e\} \tag{18}$$

where, the different $[B_i]$ matrices (i = *tb, rb, ts* and *rs*) are given in the Appendix-B (Eq. (B-3)). Therefore Eqs. (12) and (13) can be re-written as

$$\left\{\varepsilon_b^{fg}\right\}=[B_{tb}]\{d_t^e\}+[Z_1][B_{rb}]\{d_r^e\};\left\{\varepsilon_b^{P}\right\}=[B_{tb}]\{d_t^e\}+[Z_2][B_{rb}]\{d_r^e\};$$
$$\left\{\varepsilon_s^{fg}\right\}=[B_{ts}]\{d_t^e\}+[Z_3][B_{rs}]\{d_r^e\};\left\{\varepsilon_s^{Vis}\right\}=[B_{ts}]\{d_t^e\}+[Z_4][B_{rs}]\{d_r^e\}$$
$$\left\{\varepsilon_s^{P}\right\}=[B_{ts}]\{d_t^e\}+[Z_5][B_{rs}]\{d_r^e\} \tag{19}$$

2.4. Governing equations

The governing equations of motion for ACLD treated FGSMEE plate are derived by considering first variations of total potential energy (δT_p) and kinetic energy (δT_k) and employing the Hamilton's principle as follows [59]:

$$\delta T_\mathrm{p}+\delta T_\mathrm{k}=0 \tag{20}$$

The total potential energy (δT_p) of the overall system can be given by,

$$\delta T_\mathrm{p}=\delta T_{\mathrm{p\_}S}+\delta T_{\mathrm{p\_}V}+\delta T_{\mathrm{p\_}P} \tag{21}$$

where, $\delta T_{\mathrm{p\_}S}$, $\delta T_{\mathrm{p\_}V}$ and $\delta T_{\mathrm{p\_}P}$ are the potential energy of the FGSMEE substrate, the viscoelastic layer and the 1–3 PZC patch, respectively. Further, each term can be expressed as follows [48,49]:

$$\delta T_{\mathrm{p\_}S}=\int_{\Omega^k}\delta\left\{\varepsilon_b^{fg}\right\}^{\mathrm{T}}\left\{\sigma_b^{fg}\right\}\mathrm{d}\Omega^k+\int_{\Omega^k}\delta\left\{\varepsilon_s^{fg}\right\}^{\mathrm{T}}\left\{\sigma_s^{fg}\right\}\mathrm{d}\Omega^k+\int_A Q^\varphi\delta\varphi\mathrm{d}A+\int_A Q^\psi\delta\psi\mathrm{d}A-$$
$$\int_{\Omega^k}\delta E_zD_z(z)\mathrm{d}\Omega^k-\int_{\Omega^k}\delta H_zB_z(z)\mathrm{d}\Omega^k-\int_A\delta\{d_t\}^{\mathrm{T}}\{f\}\mathrm{d}A \tag{22}$$

Since the thickness of the viscoelastic layer considered is very small compared to the thickness of other layers and its axial elastic constants are much lower than that of the other layers, the strain energy of this layer corresponding to the normal strains is negligible.

$$\delta T_{\mathrm{p\_}V}=\int_{\Omega^V}\delta\left\{\varepsilon_s^{Vis}\right\}^{\mathrm{T}}\left\{\sigma_s^{Vis}\right\}\mathrm{d}\Omega^V \tag{23}$$

$$\delta T_{\mathrm{p\_}P}=\int_{\Omega^P}\delta\left\{\varepsilon_b^{P}\right\}^{\mathrm{T}}\left\{\sigma_b^{P}\right\}\mathrm{d}\Omega^P+\int_{\Omega^P}\delta\left\{\varepsilon_s^{P}\right\}^{\mathrm{T}}\left\{\sigma_s^{P}\right\}\mathrm{d}\Omega^P-\int_{\Omega^P}\delta E_zD_z\mathrm{d}\Omega^P \tag{24}$$

in which, Ω^k, Ω^V and Ω^P represents the volume of the FGSMEE substrate layer, viscoelastic and 1–3 PZC patch, respectively. Q^φ and Q^ψ are the surface electric and magnetic charge densities, respectively. Further, $\{f\}$ is the traction load vector and V refers to the voltage supplied to 1–3 PZC patch.

By substituting the constitutive equations (Eq. (1)), strain-displacement relations (Eq. (19)) and other FE parameters (Eqs. (14)–(17)) in Eq. (21), the total potential energy can be re-written as follows:

$$\begin{aligned}\delta T_{\mathrm{p\_}S}=&\int_{\Omega^k}\delta\left([B_{tb}]\{d_t^e\}+[Z_1][B_{rb}]\{d_r^e\}\right)^{\mathrm{T}}\times\left[\left[\overline{C}_b^{fg}(z)\right]\{[B_{tb}]\{d_t^e\}\right.\\&+[Z_1][B_{rb}]\{d_r^e\}\}+\left\{e_b^{fg}(z)\right\}\frac{1}{H}[N_\varphi]\{\varphi\}\\&\left.+\left\{q_b^{fg}(z)\right\}\frac{1}{H}[N_\psi]\{\psi\}\right]\mathrm{d}\Omega^k+\int_{\Omega^k}\delta\left([B_{ts}]\{d_t^e\}+[Z_3][B_{rs}]\{d_r^e\}\right)^{\mathrm{T}}\\&\times\left[\left[\overline{C}_s^{fg}(z)\right]\left([B_{ts}]\{d_t^e\}+[Z_3][B_{rs}]\{d_r^e\}\right)\right]\mathrm{d}\Omega^k\\&+\int_{\Omega^k}\delta\left[\frac{1}{H}\{\varphi^e\}^{\mathrm{T}}[N_\varphi]^{\mathrm{T}}\right]\times\left[\left\{e_b^{fg}(z)\right\}^{\mathrm{T}}\left([B_{tb}]\{d_t^e\}+[Z_1][B_{rb}]\{d_r^e\}\right)\right.\\&-\left.\in_{33}^{fg}(z)\left(\frac{1}{H}[N_\varphi]\{\varphi^e\}\right)-d_{33}^{fg}(z)\left(\frac{1}{H}[N_\psi]\{\psi^e\}\right)\right]\mathrm{d}\Omega^k\\&+\int_{\Omega^k}\delta\left[\frac{1}{H}\{\psi^e\}^{\mathrm{T}}[N_\psi]^{\mathrm{T}}\right]\times\left[\left\{q_b^{fg}(z)\right\}^{\mathrm{T}}\left([B_{tb}]\{d_t^e\}+[Z_1][B_{rb}]\{d_r^e\}\right)\right.\\&\left.-d_{33}^{fg}(z)\left(\frac{1}{H}[N_\varphi]\{\varphi^e\}\right)-\mu_{33}^{fg}(z)\left(\frac{1}{H}[N_\psi]\{\psi^e\}\right)\right]\mathrm{d}\Omega^k\\&-\int_A\delta\{d_t\}^{\mathrm{T}}\{f\}\mathrm{d}A+\int_A Q^\varphi\delta[N_\varphi]\{\varphi\}\mathrm{d}A+\int_A Q^\psi\delta[N_\psi]\{\psi\}\mathrm{d}A\end{aligned} \tag{25}$$

$$\delta T_{p\_V} = \int_{\Omega^V} \delta\left([B_{ts}]\{d_t^e\} + [Z_4][B_{rs}]\{d_r^e\}\right)^T \left[\left[\overline{C}_s^V\right]\left([B_{ts}]\{d_t^e\} + [Z_4][B_{rs}]\{d_r^e\}\right)\right] d\Omega^V$$

$$\delta T_{p\_P} = \int_{\Omega^P} \delta\left([B_{tb}]\{d_t^e\} + [Z_2][B_{rb}]\{d_r^e\}\right)^T \times \left[\left[\overline{C}_b^P\right]\left([B_{tb}]\{d_t^e\} + [Z_2][B_{rb}]\{d_r^e\}\right) + \left[\overline{C}_{bs}^P\right]\left([B_{ts}]\{d_t^e\} + [Z_5][B_{rs}]\{d_r^e\}\right) + \frac{1}{h_p}\left\{e_b^p\right\}V\right] d\Omega^P \quad (26)$$

$$\int_{\Omega^P} \delta\left([B_{ts}]\{d_t^e\} + [Z_5][B_{rs}]\{d_r^e\}\right)^T \times \left[\left[\overline{C}_{bs}^P\right]^T\left([B_{tb}]\{d_t^e\} + [Z_2][B_{rb}]\{d_r^e\}\right) + \left[\overline{C}_s^P\right]\left([B_{ts}]\{d_t^e\} + [Z_5][B_{rs}]\{d_r^e\}\right) + \frac{1}{h_p}\{e_s^p\}V\right] d\Omega^P \quad (27)$$

Assigning different rigidity matrices, stiffness matrices and force vectors, Eqs. (25)–(27) can be represented as follows:

$$\begin{aligned}
\delta T_p = {} & \delta\{d_t^e\}^T\left([K_{ttc}^e] + [K_{tsv}^e] + \left[K_{tbp}^e\right] + \left[K_{tsp}^e\right]\right)\{d_t^e\} + \\
& \delta\{d_t^e\}^T\left([K_{trc}^e] + [K_{trsv}^e] + \left[K_{trbp}^e\right] + \left[K_{trsp}^e\right]\right)\{d_r^e\} + \\
& \delta\{d_r^e\}^T\left([K_{trc}^e]^T + [K_{trsv}^e]^T + \left[K_{trbp}^e\right]^T + \left[K_{trsp}^e\right]^T\right)\{d_t^e\} + \\
& \delta\{d_r^e\}^T\left([K_{rrc}^e] + [K_{rrsv}^e] + \left[K_{rrbp}^e\right] + \left[K_{rrsp}^e\right]\right)\{d_r^e\} + \\
& \delta\{d_t^e\}^T[K_{t\varphi}^e]\{\varphi^e\} + \delta\{d_r^e\}^T[K_{r\varphi}^e]\{\varphi^e\} + \delta\{d_t^e\}^T[K_{t\psi}^e]\{\psi^e\} + \delta\{d_r^e\}^T[K_{r\psi}^e]\{\psi^e\} + \\
& \delta\{\varphi^e\}^T\left([K_{t\varphi}^e]^T\{d_t^e\} + [K_{r\varphi}^e]^T\{d_r^e\} - [K_{\varphi\varphi}^e]\{\varphi^e\} - [K_{\varphi\psi}^e]\{\psi^e\}\right) + \\
& \delta\{\psi^e\}^T\left([K_{t\psi}^e]^T\{d_t^e\} + [K_{r\psi}^e]^T\{d_r^e\} - [K_{\psi\varphi}^e]\{\varphi^e\} - [K_{\psi\psi}^e]\{\psi^e\}\right) - \delta\{\varphi^e\}^T\{F_\varphi\} - \\
& \delta\{\psi^e\}^T\{F_\psi\} - \delta\{d_t^e\}^T\{F_t^e\} + \delta\{d_t^e\}^T\left[\left\{F_{tpb}^e\right\} + \left\{F_{tps}^e\right\}\right]V + \delta\{d_r^e\}^T\left[\left\{F_{rpb}^e\right\} + \left\{F_{rps}^e\right\}\right]V
\end{aligned} \quad (28)$$

The explicit representation of various coupled stiffness matrices and force vectors appearing in Eq. (28) are depicted in Appendix-C. Analogously, the kinetic energy of the typical element of ACLD-FGSMEE plate can be given by,

$$\delta T_k^e = \frac{1}{2}\int_{\Omega^k} \delta\{d_t\}^T \rho_{fg}(z)\{\ddot{d}_t\} d\Omega^k + \frac{1}{2}\int_{\Omega^V} \delta\{d_t\}^T \rho_V\{\ddot{d}_t\} d\Omega^V + \frac{1}{2}\int_{\Omega^P} \delta\{d_t\}^T \rho_P\{\ddot{d}_t\} d\Omega^P \delta T_k^e = \frac{1}{2}\{d_t^e\}^T[M^e]\{\ddot{d}_t^e\} \quad (29)$$

The elemental equations of motion for the overall ACLD treated FGSMEE plate is obtained through condensation technique [59]:

$$\begin{aligned}
& [M^e]\{\ddot{d}_t^e\} + [K_{tt}^e]\{d_t^e\} + [K_{tr}^e]\{d_r^e\} + [K_{t\varphi}^e]\{\varphi^e\} + [K_{t\psi}^e]\{\psi^e\} \\
& = \{F^e\} - \left\{F_{tp}^e\right\}V \\
& [K_{tr}^e]^T\{d_t^e\} + [K_{rr}^e]\{d_r^e\} + [K_{r\varphi}^e]\{\varphi^e\} + [K_{r\psi}^e]\{\psi^e\} = -\left\{F_{rp}^e\right\}V \\
& [K_{t\varphi}^e]^T\{d_t^e\} + [K_{r\varphi}^e]^T\{d_r^e\} - [K_{\varphi\varphi}^e]\{\varphi^e\} - [K_{\varphi\psi}^e]\{\psi^e\} = \{F_\varphi^e\} \\
& [K_{t\psi}^e]^T\{d_t^e\} + [K_{r\psi}^e]^T\{d_r^e\} - [K_{\varphi\psi}^e]^T\{\varphi^e\} - [K_{\psi\psi}^e]\{\psi^e\} = \{F_\psi^e\}
\end{aligned} \quad (30)$$

2.5. Skew boundary transformation

The transformed displacement components of the nodes lying on the skew edges with respect to transformed axes x'-, y'- and z'- can be represented as follows:

$$\{d_t\} = [L_t]\left\{d_t^1\right\}; \{d_r\} = [L_r]\left\{d_r^1\right\} \quad (31)$$

where, $\{d_t^1\}$ and $\{d_r^1\}$ are the transformed displacement components which can be given by

$$\left\{d_t^1\right\} = \left[u_0^1 \;\; v_0^1 \;\; w_0^1\right]^T; \left\{d_r^1\right\} = \left[\theta_x^1 \;\; \theta_y^1 \;\; \theta_z^1 \;\; \kappa_z^1 \;\; \kappa_x^1 \;\; \kappa_y^1 \;\; \gamma_x^1 \;\; \gamma_y^1\right]^T \quad (32)$$

Further, $[L_t]$ and $[L_r]$ the transformation matrices which can be expressed as [59].

$$[L_t]=\begin{bmatrix} c & s & 0 \\ -s & c & 0 \\ 0 & 0 & 1 \end{bmatrix};\ [L_r]=\begin{bmatrix} c & s & 0 & 0 & 0 & 0 & 0 & 0 \\ -s & c & 0 & 0 & 0 & 0 & 0 & 0 \\ 0 & 0 & 1 & 0 & 0 & 0 & 0 & 0 \\ 0 & 0 & 0 & c & s & 0 & 0 & 0 \\ 0 & 0 & 0 & -s & c & 0 & 0 & 0 \\ 0 & 0 & 0 & 0 & 0 & 1 & 0 & 0 \\ 0 & 0 & 0 & 0 & 0 & c & s & 0 \\ 0 & 0 & 0 & 0 & 0 & -s & c & 0 \end{bmatrix} \tag{33}$$

where, $c=\cos\lambda$ and $s=\sin\lambda$. With this transformation, the coupled elemental stiffness matrices having atleast one node existing on the transformed skew edge may be given by

$$[\overline{K_{tt}^e}]=[T_1]^{\mathrm{T}}[K_{tt}^e][T_1];\ [\overline{K_{tr}^e}]=[T_1]^{\mathrm{T}}[K_{tr}^e][T_2];$$

$$[\overline{K_{rr}^e}]=[T_2]^{\mathrm{T}}[K_{rr}^e][T_2];\ [\overline{M^e}]=[T_1]^{\mathrm{T}}[M^e][T_1];$$

$$[T_1]=\begin{bmatrix} [L_t] & \bar{o} & \bar{o} & \bar{o} & \bar{o} & \bar{o} & \bar{o} & \bar{o} \\ \bar{o} & [L_t] & \bar{o} & \bar{o} & \bar{o} & \bar{o} & \bar{o} & \bar{o} \\ \bar{o} & \bar{o} & [L_t] & \bar{o} & \bar{o} & \bar{o} & \bar{o} & \bar{o} \\ \bar{o} & \bar{o} & \bar{o} & [L_t] & \bar{o} & \bar{o} & \bar{o} & \bar{o} \\ \bar{o} & \bar{o} & \bar{o} & \bar{o} & [L_t] & \bar{o} & \bar{o} & \bar{o} \\ \bar{o} & \bar{o} & \bar{o} & \bar{o} & \bar{o} & [L_t] & \bar{o} & \bar{o} \\ \bar{o} & \bar{o} & \bar{o} & \bar{o} & \bar{o} & \bar{o} & [L_t] & \bar{o} \\ \bar{o} & \bar{o} & \bar{o} & \bar{o} & \bar{o} & \bar{o} & \bar{o} & [L_t] \end{bmatrix} \tag{34}$$

$$[T_2]=\begin{bmatrix} [L_r] & \bar{\bar{o}} & \bar{\bar{o}} & \bar{\bar{o}} & \bar{\bar{o}} & \bar{\bar{o}} & \bar{\bar{o}} & \bar{\bar{o}} \\ \bar{\bar{o}} & [L_r] & \bar{\bar{o}} & \bar{\bar{o}} & \bar{\bar{o}} & \bar{\bar{o}} & \bar{\bar{o}} & \bar{\bar{o}} \\ \bar{\bar{o}} & \bar{\bar{o}} & [L_r] & \bar{\bar{o}} & \bar{\bar{o}} & \bar{\bar{o}} & \bar{\bar{o}} & \bar{\bar{o}} \\ \bar{\bar{o}} & \bar{\bar{o}} & \bar{\bar{o}} & [L_r] & \bar{\bar{o}} & \bar{\bar{o}} & \bar{\bar{o}} & \bar{\bar{o}} \\ \bar{\bar{o}} & \bar{\bar{o}} & \bar{\bar{o}} & \bar{\bar{o}} & [L_r] & \bar{\bar{o}} & \bar{\bar{o}} & \bar{\bar{o}} \\ \bar{\bar{o}} & \bar{\bar{o}} & \bar{\bar{o}} & \bar{\bar{o}} & \bar{\bar{o}} & [L_r] & \bar{\bar{o}} & \bar{\bar{o}} \\ \bar{\bar{o}} & \bar{\bar{o}} & \bar{\bar{o}} & \bar{\bar{o}} & \bar{\bar{o}} & \bar{\bar{o}} & [L_r] & \bar{\bar{o}} \\ \bar{\bar{o}} & \bar{\bar{o}} & \bar{\bar{o}} & \bar{\bar{o}} & \bar{\bar{o}} & \bar{\bar{o}} & \bar{\bar{o}} & [L_r] \end{bmatrix}$$

in which, $\bar{o}$ and $\bar{\bar{o}}$ are null matrices of size (3 × 3) and (8 × 8), respectively.

Once the transformations have been carried out, the coupled equilibrium equation of motion of ACLD-FGSMEE plate can be expressed in the global form as follows [57,59]:

$$[M]\{\ddot{X}\}+[K_{tt}]\{X\}+[K_{tr}]\{X_r\}+[K_{t\varphi}]\{\varphi\}+[K_{t\psi}]\{\psi\}=\{F\}-\sum_{l=1}^{m}\left(\left\{F_{tp}^l\right\}\right)V^l \tag{35a}$$

$$[K_{tr}]^{\mathrm{T}}\{X\}+[K_{rr}]\{X_r\}+[K_{r\varphi}]\{\varphi\}+[K_{r\psi}]\{\psi\}=-\sum_{l=1}^{m}\left\{F_{rp}^l\right\}V^l \tag{35b}$$

$$[K_{t\varphi}]^{\mathrm{T}}\{X\}+[K_{r\varphi}]^{\mathrm{T}}\{X_r\}-[K_{\varphi\varphi}]\{\varphi\}-[K_{\varphi\psi}]\{\psi\}=\{F_\varphi\} \tag{35c}$$

$$[K_{t\psi}]^{\mathrm{T}}\{X\}+[K_{r\psi}]^{\mathrm{T}}\{X_r\}-[K_{\varphi\psi}]^{\mathrm{T}}\{\varphi\}-[K_{\psi\psi}]\{\psi\}=\{F_\psi\} \tag{35d}$$

where, $[M]$ is the global mass matrix; $[K_{tt}]$, $[K_{tr}]$ and $[K_{rr}]$ are global elastic stiffness matrices; $[K_{t\varphi}]$ and $[K_{r\varphi}]$ are the global coupled electro-elastic stiffness matrices; $[K_{t\psi}]$ and $[K_{r\psi}]$ are coupled magneto-elastic stiffness matrices; $[K_{\psi\psi}]$ and $[K_{\varphi\varphi}]$ magnetic and electric stiffness matrices, respectively; $\{F\}$ and is the mechanical force vectors; $\{F_\varphi\}$ and $\{F_\psi\}$ are the electrical force vector and magnetic force vector, respectively. Meanwhile, m denotes total number of patches and V^l indicates the magnitude of the voltage applied to the lth patch.

Further, for the closed-loop model, a simple derivative control law has been adopted. Therefore, control voltage can be explicitly expressed in terms of the derivative of global nodal degrees of freedom as follows:

$$V^l=-K_d^l\dot{w}_0(x_l,y_l)=-K_d^l\left[U_t^l\right]\{\dot{X}\} \tag{36}$$

$[U_t^l]$ is the transverse velocity unit vectors. K_d^l is the control gain of the ACLD patch. Substituting Eq. (36) in Eq. (31) yields

$$\begin{aligned} &[M]\{\ddot{X}\}+[K_{tt}]\{X\}+[K_{tr}]\{X_r\}+[K_{t\varphi}]\{\varphi\}+[K_{t\psi}]\{\psi\} \\ &=\sum_{l=1}^{m}\left(\left\{F_{tp}^l\right\}\right)K_d^l\left[U_t^l\right]\{\dot{X}\}+\{F\} \\ &[K_{tr}]^T\{X\}+[K_{rr}]\{X_r\}+[K_{r\varphi}]\{\varphi\}+[K_{r\psi}]\{\psi\}=\sum_{l=1}^{m}\left(\left\{F_{rp}^l\right\}\right)K_d^l\left[U_t^l\right]\{\dot{X}\} \\ &[K_{t\varphi}]^T\{X\}+[K_{r\varphi}]^T\{X_r\}-[K_{\varphi\varphi}]\{\varphi\}-[K_{\varphi\psi}]\{\psi\}=\{F_\varphi\} \\ &[K_{t\psi}]^T\{X\}+[K_{r\psi}]^T\{X_r\}-[K_{\varphi\psi}]^T\{\varphi\}-[K_{\psi\psi}]\{\psi\}=\{F_\psi\} \end{aligned} \tag{37}$$

Table 2
Corroboration of the natural frequencies utilizing the present FE formulation.

Stacking Sequence	Mode No.	Non-Dimensional Frequency		% Error
		Chen et al. [24]	Present	
BFB	1	1.3434	1.3482	0.356
	2	2.2199	2.2279	0.359
	3	2.2199	2.2279	0.359
FBF	1	1.4463	1.4346	−0.815
	2	2.3602	2.3390	−0.906
	3	2.3602	2.3392	−0.897

% Error = (Present Value - Value reported in Chen et al. [24])/Present Value.

3. Results and discussion

This section presents a series of illustrations are to clarify the effect of ACLD treatment on the controlled linear frequency behavior of FGSMEE plates through the FE formulation derived in the previous section. A converged 10 × 10 FE mesh discretised by an eight noded isoparametric quadrilateral element is utilized in this study. The present analysis considers the geometry of the FGSMEE plates to be $a=b=0.5$ m; and $a/H=100$. In order to facilitate numerical evaluation, the thicknesses of 50.8 μm and 250 μm are assigned to the visco-elastic layer and the 1–3 PZC layer, respectively. An actuating force of 2 N is applied at ($a/2$, $b/4$ Cos λ, $H/2$) to excite the first few modes of the FGSMEE plate. In addition, the details of viscoelastic layers can be illustrated as follows [61]:

Complex shear modulus, $G=20(1+i)$ MN/m^2; Poisson's Ratio, $\nu=0.49$; Density, $\rho_v=1140$ kg/m^3. Meanwhile, the skew boundary constraints enforced in the present analysis can be illustrated as follows:

Table 3
Non-dimensional frequency parameter for the clamped-clamped laminated composite skew plate ($a/h = 10$).

Skew angle (λ)	Source	Antisymmetric cross-ply ($0^0/90^0/0^0/90^0$)			Antisymmetric angle-ply ($45^0/-45^0/45^0/-45^0$)			Symmetric cross-ply ($90^0/0^0/90^0/0^0/90^0$)		
		Modes			Modes			Modes		
		1	2	3	1	2	3	1	2	3
0^0	Kanasogi and Ray [55]	2.2990	3.7880	3.7880	2.2119	3.7339	3.7339	2.3687	3.5399	4.1122
	Present	2.2990	3.5913	3.8695	2.1767	3.5746	3.5139	2.3400	3.3655	4.2382
15^0	Kanasogi and Ray [55]	2.3809	3.7516	4.0785	2.3099	3.6997	4.0438	2.4663	3.6255	4.3418
	Present	2.3992	3.5560	4.0841	2.2344	3.5111	3.9290	2.3160	3.4637	4.2346
30^0	Kanasogi and Ray [55]	2.6666	3.9851	4.7227	2.6325	3.9549	5.2107	2.7921	3.9557	5.0220
	Present	2.4903	3.8967	4.4609	2.4722	3.5807	5.0199	2.4896	3.6363	4.7949
45^0	Kanasogi and Ray [55]	3.3015	4.6290	5.8423	3.3015	4.6290	5.8423	3.4739	4.7129	5.8789
	Present	2.7948	4.5102	5.6270	2.8348	4.5102	5.4970	2.9439	4.6545	5.4362

$$v_0^1 = w_0^1 = \theta_y^1 = \kappa_y^1 = \gamma_y^1 = \theta_z^1 = \kappa_z^1 = 0 \text{ at } x = y\tan\lambda \text{ and } x = a + y\tan\lambda \tag{38}$$

$$u_0 = w_0 = \theta_x = \kappa_x = \gamma_x = \theta_z = \kappa_z = 0 \text{ at } y = 0 \text{ and } y = b\cos\lambda.$$

3.1. Verification of the FE model

The results obtained through the FE formulation proposed in the present work are verified for its correctness with the previous published articles. In this regard, the FGSMEE plate is reduced to layered MEE plate. Therefore, the material properties are reduced to homogeneous material by setting the power-law index to 0 and ∞ to obtain homogeneous B and F layer, respectively. A comparison is made between the results obtained for layered MEE plates through the current FE formulation and the results mentioned by Chen et al. [24]. In this regard, the ACLD effect is neglected. The similarity between the compared results is reflected in Table 2. An extended verification is illustrated in Table 3 to justify the procedure adopted for skew edge transformation. To this end, the numerical problem of skew composite plates posed in Ref. [55] is resolved once again via present method. The effectiveness of this formulation is evident from the minimal discrepancies between the results as shown in Table 3. Therefore, an extension of the current formulation can be made to assess the FGSMEE plates with ACLD.

The effect of skewness on the frequency response of the plates is illustrated in Fig. 2(a) and (b). It is crucial to point out that a remarkable reduction in the transverse deflection (w) and the control voltage can be noticed with increasing skew angles. The reason is due to the fact that with higher skewness of the plate, the plate area reduces which inturn enhances the stiffness of the plate. According to the diagrams, it can also be observed that among the two forms of functional gradation considered, 'B' rich bottom yields a lesser magnitude of the transverse deflection (w) and the control voltage in contrast to 'F' rich bottom. It may be due to the fact that the excitation load is applied on the top surface of the plate and for FGSMEE plate made of 'B' rich bottom, the stiffness gradually increases towards the top surface as the percentage of 'F' with higher elastic coefficient improves. In turn the resistance to deflection rises. Therefore, a slightly greater attenuation capacity is witnessed for FGSMEE plate made of 'B' rich bottom. Based on the figure, it can be concluded that FGSMEE with a higher skew angle and 'B' rich bottom material distribution results in higher attenuation of frequency response and requires minimal control voltage to accomplish it.

Fig. 3(a) and (b) are devoted to plot the disparities in the deflection w and requisite control voltages of FGSMEE plates with different power-law indices. As witnessed in these figures, the increasing power-law index 'r', results in an effective improvement in the attenuation capability. As the power-law index 'r' improves, the predominant influence of pure piezomagnetic phases (F) in the overall FG composition increases. Therefore, the stiffness of the FGSMEE plate enhances which reduces the deflection of the plate. It holds good for both 'B' rich bottom and 'F' rich bottom material distributions. On the other hand, the impact of coupling fields on the frequency response of FGSMEE plate is illustrated in Fig. (4) considering $r = 0.5$ and 'B' rich Bottom material distribution. As inferred from this figure, the coupled interaction results in reduced value of w and control voltage as opposed to the frequency response neglecting coupling (considering only the elastic fields). This is due to the additional contribution of coupled stiffness to the overall stiffness of the FGSMEE plate. Furthermore, considering the coupling effects, the variation of transverse deflection and control voltage with different power-law index and skew angles are illustrated in Tables 4 and 5, respectively.

Fig. 5(a) contrasts between the frequency response of FGSMEE plates controlled with ACLD and uncontrolled state. 'B' rich Bottom material distribution and $r = 1.0$ is considered for this study. It can be inferred from this figure that incorporating ACLD treatment results in a drastic reduction of the amplitude of vibration. On these grounds, the study is extended to evaluate the effect of control gain (K_d) on the damping behavior of FGSMEE plate. Based on Fig. 5(b) and Table 6 it is clear that a higher control gain has a noteworthy effect on the controlled response of FGSMEE plate due to improved damping force produced.

Meanwhile, the influence of patch locations is studied considering two variants of patch positions. The first corresponds to the two end patches (EP) embedded at two ends of the FGSMEE plate as depicted in Fig. 1(a). Analogously, the second corresponds to the single centre patch (CP) placed at the centre of FGSMEE plate Fig. 1(b). Fig. 6(a) and (b) show the effect of patch position on FGSMEE plate ('F' rich bottom material distribution) for different skew angle and power-law index. As same as former diagrams, a significant influence of using higher skew angle and power-law index is witnessed here as well. Alongside, based on the diagrams it can be highlighted that irrespective of the skew angle and power-law index, the centre patch has a predominant effect on vibration attenuation. This may be due to the fact that the EP is nearer to the plate edges which are already constrained. Therefore, the contribution of EP in improving the plate's stiffness is minimal. Meanwhile, the CP improves the stiffness of the plate along in addition to the constraints provided at the edges. This leads to reduced vibration in contrast to the EP. Tables 7 and 8 encapsulate the combined influences of all these parameters along with the patch positions on the maximum values of w and control voltage of

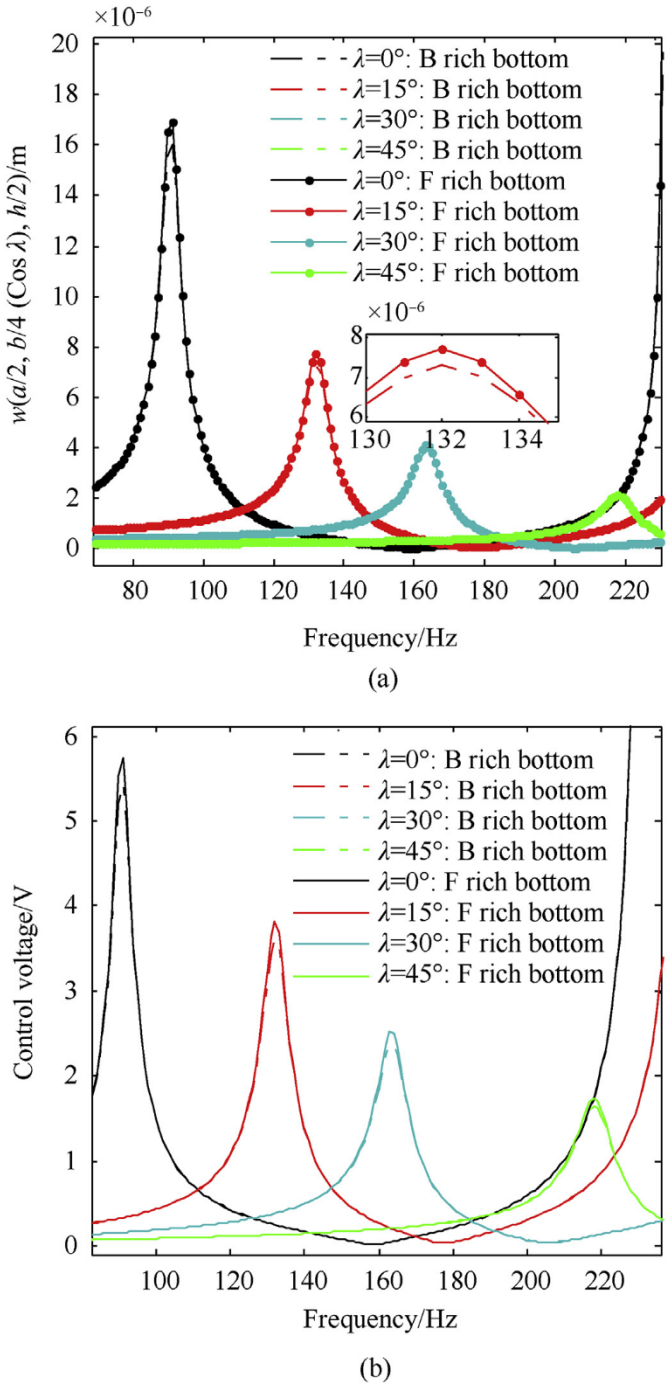

Fig. 2. Effect of skew angles on the (a) transverse deflection '*w*' and(b) control voltage (r = 0.5; centre patch; K_d = 600).

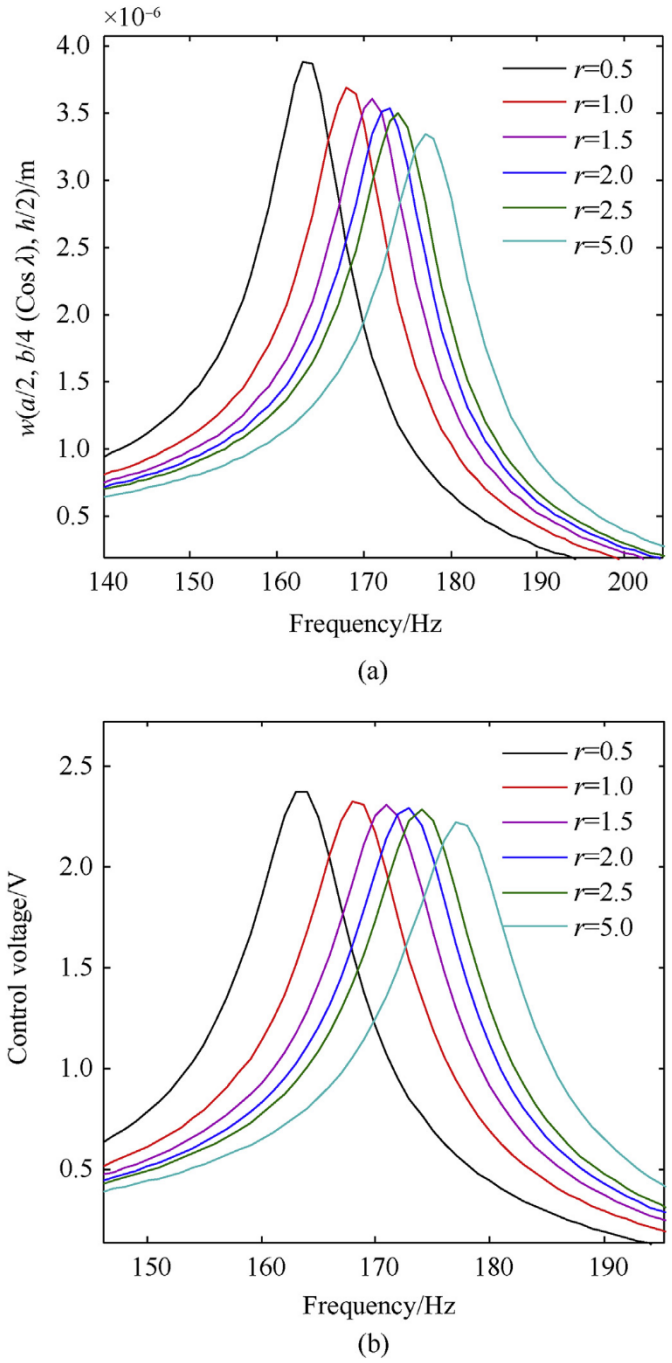

Fig. 3. Influence of power-law index on (a) transverse deflection *w* and (b) control voltage (λ = 30°; B rich bottom; centre patch; K_d = 600).

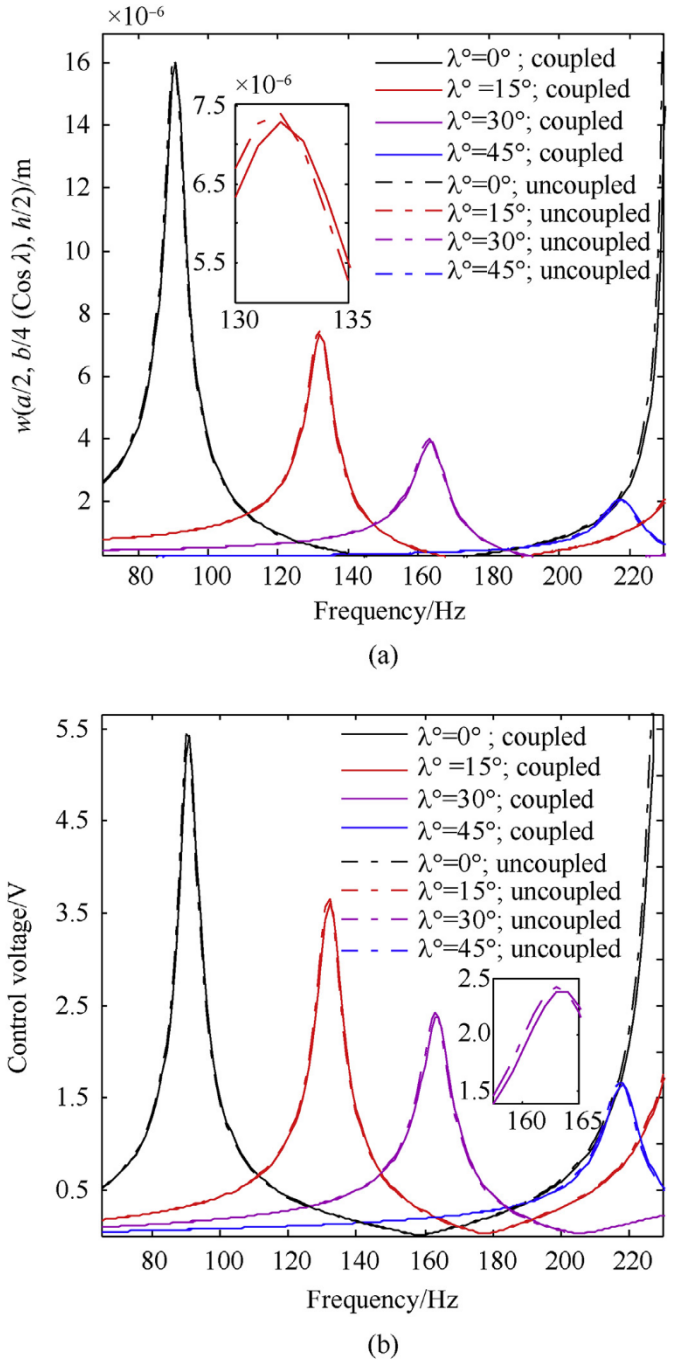

Fig. 4. Influence of coupling on (a) transverse deflection w and (b) control voltage ($r = 1$; B rich bottom; centre patch; $K_d = 600$).

Table 4
Effect of skew angle, power-law index, coupling on the transverse deflection w ($\times 10^{-5}$ m).

Power-Law index	Skew Angle	B rich Bottom		F rich Bottom	
		Coupled	Uncoupled	Coupled	Uncoupled
$r = 0.5$	0	1.60	1.68	1.69	1.7576
	15	0.73	0.76	0.77	0.800
	30	0.38	0.39	0.41	0.4264
	45	0.19	0.20	0.21	0.2184
$r = 1$	0	1.50	1.57	1.60	1.664
	15	0.69	0.72	0.735	0.7644
	30	0.37	0.38	0.392	0.40768
	45	0.19	0.19	0.201	0.20904
$r = 1.5$	0	1.49	1.56	1.58	1.6432
	15	0.67	0.71	0.717	0.74568
	30	0.36	0.37	0.382	0.39728
	45	0.18	0.19	0.196	0.20384
$r = 2$	0	1.47	1.54	1.55	1.612
	15	0.66	0.71	0.706	0.73424
	30	0.351	0.36	0.372	0.38688
	45	0.182	0.191	0.192	0.19968
$r = 2.5$	0	1.45	1.52	1.517	1.57768
	15	0.64	0.69	0.694	0.72176
	30	0.35	0.37	0.36	0.3744
	45	0.17	0.18	0.188	0.19552
$r = 5$	0	1.38	1.449	1.42	1.4768
	15	0.63	0.6615	0.65	0.676
	30	0.33	0.3507	0.345	0.3588
	45	0.16	0.1806	0.177	0.18408

Table 5
Effect of skew angle, power-law index, coupling on the control voltage (in Volts).

Power-Law index	Skew Angle	B rich bottom		F rich bottom	
		Coupled	Uncoupled	Coupled	Uncoupled
$r = 0.5$	0	5.43	5.59	5.743	5.97
	15	3.6	3.70	3.814	3.96
	30	2.38	2.45	2.513	2.61
	45	1.62	1.66	1.743	1.82
$r = 1$	0	5.32	5.48	5.61	5.83
	15	3.52	3.63	3.74	3.89
	30	2.36	2.43	2.473	2.57
	45	1.606	1.65	1.704	1.77
$r = 1.5$	0	5.29	5.45	5.59	5.81
	15	3.5	3.61	3.706	3.85
	30	2.34	2.41	2.45	2.55
	45	1.58	1.62	1.68	1.74
$r = 2$	0	5.26	5.42	5.55	5.77
	15	3.48	3.58	3.67	3.82
	30	2.30	2.37	2.42	2.52
	45	1.56	1.61	1.66	1.73
$r = 2.5$	0	5.236	5.39	5.492	5.72
	15	3.468	3.57	3.64	3.79
	30	2.28	2.35	2.395	2.50
	45	1.55	1.59	1.641	1.71
$r = 5$	0	5.11	5.26	5.26	5.48
	15	3.37	3.47	3.48	3.6192
	30	2.22	2.28	2.29	2.3816
	45	1.53	1.58	1.58	1.6432

FGSMEE plate, respectively.

Furthermore, the analysis is extended to investigate the effects of piezoelectric fiber orientations of 1–3 PZC layer on the FGSMEE plate. The variation of w and control voltage illustrated in Fig. 7(a) and (b), respectively, affirm the maximum control capability of 1–3

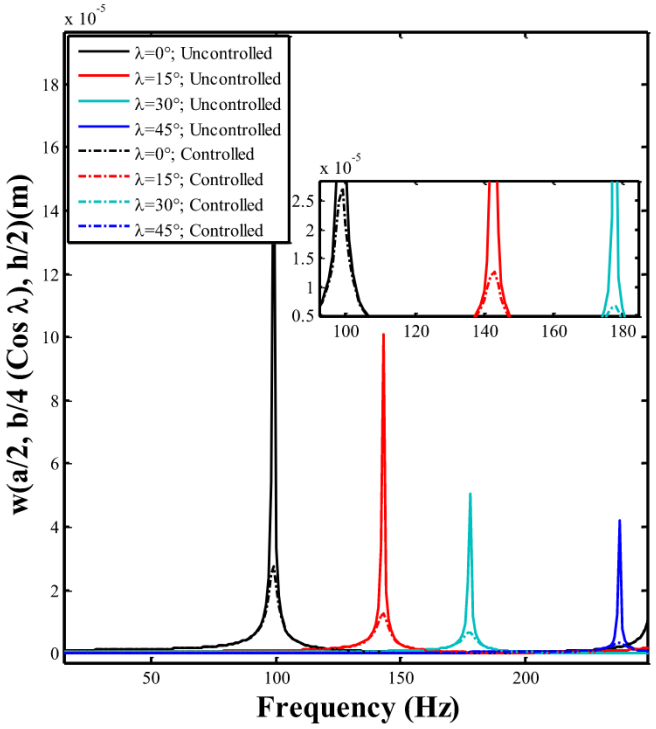

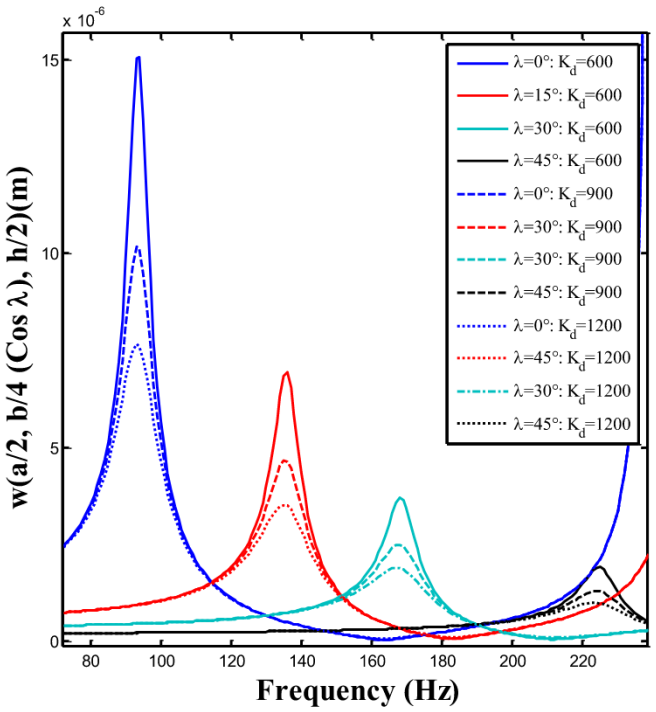

(b) $r = 1.0$, ***B*** rich bottom

Fig. 5. Variation of transverse deflection w of (a) ACLD treated and untreated FGSMEE plate (b) different control gains of ACLD.

Table 6
Effect of control gain (K_d) on the transverse deflection w ($\times 10^{-5}$ m).

Power-Law index	Skew Angle	B rich Bottom			F rich Bottom		
		$K_d = 600$	$K_d = 900$	$K_d = 1200$	$K_d = 600$	$K_d = 900$	$K_d = 1200$
$r = 1$	0	1.50	1.01	0.76	1.60	1.08	0.80
	15	0.692	0.46	0.35	0.735	0.49	0.37
	30	0.37	0.25	0.19	0.392	0.27	0.21
	45	0.189	0.13	0.09	0.201	0.14	0.11
$r = 2$	0	1.47	0.98	0.73	1.55	1.03	0.77
	15	0.669	0.43	0.33	0.706	0.46	0.35
	30	0.351	0.22	0.17	0.372	0.24	0.19
	45	0.182	0.12	0.08	0.192	0.13	0.10
$r = 5$	0	1.38	0.92	0.69	1.42	0.95	0.71
	15	0.63	0.41	0.31	0.65	0.43	0.32
	30	0.334	0.20	0.16	0.345	0.22	0.17
	45	0.17	0.10	0.07	0.177	0.11	0.09

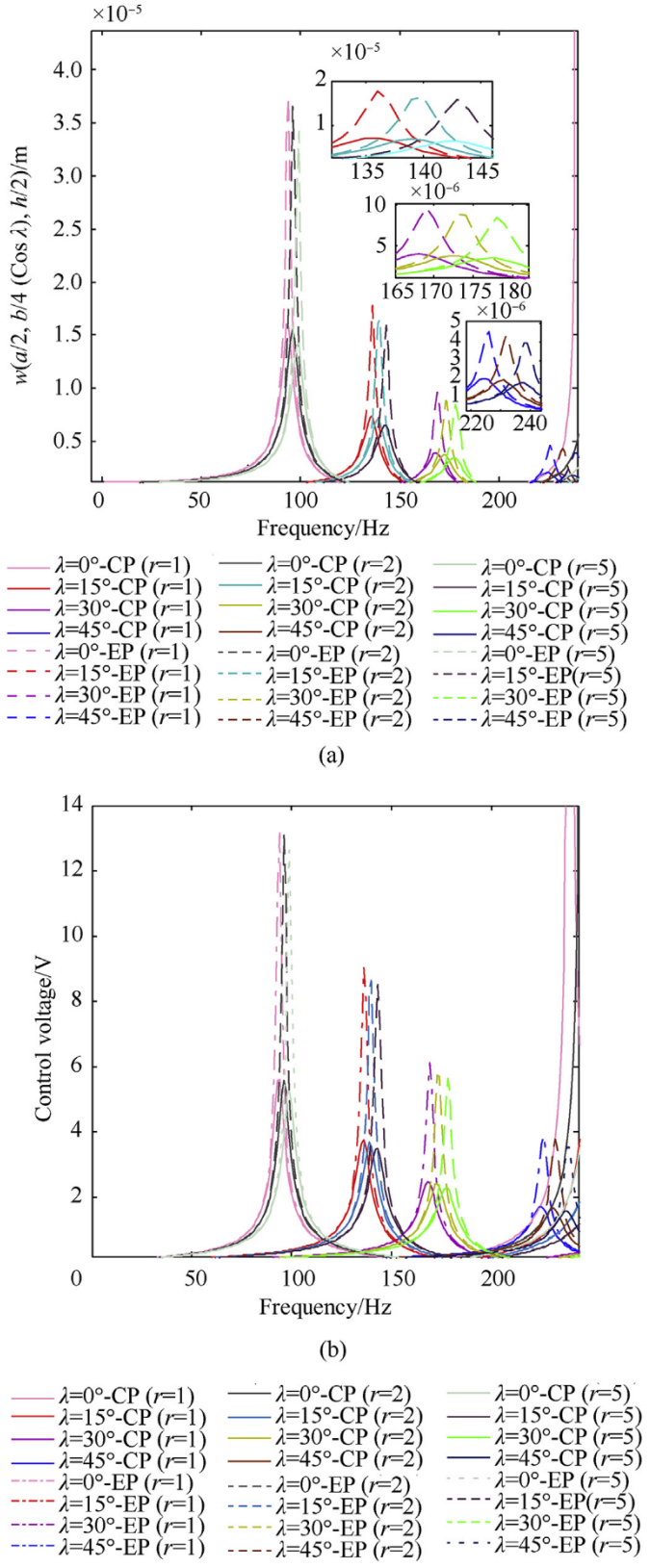

Fig. 6. Effect of patch positions on (a) transverse deflection w and (b) control voltage (F rich bottom; centre patch; $K_d = 600$).

Table 7
Effect of patch position on the required control voltage (in Volts).

Skew Angle	$r = 0.5$				$r = 1$				$r = 1.5$				$r = 2$				$r = 2.5$				$r = 5$			
	B rich bottom		F rich bottom		B rich bottom		F rich bottom		B rich bottom		F rich bottom		B rich bottom		F rich bottom		B rich bottom		F rich bottom		B rich bottom		F rich bottom	
	E.P	C.P	E.P	C.P	E.P	C.P	E.P	C.P	E.P	C.P	E.P	C.P	E.P	C.P	E.P	C.P	E.P	C.P	E.P	C.P	E.P	C.P	E.P	C.P
0	13.05	5.43	13.8	5.743	12.63	5.32	13.25	5.61	12.48	5.29	13.21	5.59	12.45	5.26	13.15	5.55	12.41	5.23	13.08	5.492	12.28	5.11	12.65	5.26
15	8.54	3.6	9.03	3.814	8.47	3.52	8.89	3.74	8.45	3.5	8.87	3.706	8.29	3.48	8.62	3.67	8.26	3.46	8.52	3.64	8.16	3.37	8.48	3.48
30	5.92	2.38	6.22	2.513	5.8	2.36	6.11	2.473	5.69	2.34	5.96	2.45	5.62	2.30	5.84	2.42	5.5	2.28	5.73	2.395	5.48	2.22	5.63	2.29
45	3.8	1.62	3.98	1.743	3.7	1.606	3.8	1.704	3.63	1.58	3.78	1.68	3.6	1.56	3.74	1.66	3.5	1.55	3.72	1.641	3.3	1.53	3.53	1.58

Table 8
Effect of patch position on the transverse deflection w ($\times 10^{-5}$ m).

Skew Angle	$r = 0.5$				$r = 1$				$r = 1.5$				$r = 2$				$r = 2.5$				$r = 5$			
	B rich bottom		F rich bottom		B rich bottom		F rich bottom		B rich bottom		F rich bottom		B rich bottom		F rich bottom		B rich bottom		F rich bottom		B rich bottom		F rich bottom	
	E.P	C.P	E.P	C.P	E.P	C.P	E.P	C.P	E.P	C.P	E.P	C.P	E.P	C.P	E.P	C.P	E.P	C.P	E.P	C.P	E.P	C.P	E.P	C.P
0	3.85	1.60	4.06	1.69	3.55	1.50	3.75	1.60	3.52	1.49	3.72	1.58	3.48	1.47	3.66	1.55	3.46	1.447	3.64	1.447	3.32	1.38	3.42	1.42
15	1.7	0.73	1.78	0.77	1.68	0.692	1.77	0.735	1.63	0.68	1.72	0.717	1.57	0.669	1.64	0.706	1.55	0.661	1.60	0.661	1.53	0.63	1.59	0.65
30	0.96	0.38	1.01	0.41	0.91	0.37	0.96	0.392	0.88	0.36	0.92	0.382	0.86	0.351	0.89	0.372	0.85	0.35	0.88	0.35	0.82	0.334	0.84	0.345
45	0.46	0.19	0.48	0.21	0.43	0.189	0.45	0.201	0.42	0.18	0.43	0.196	0.41	0.182	0.42	0.192	0.4	0.179	0.40	0.179	0.38	0.172	0.39	0.177

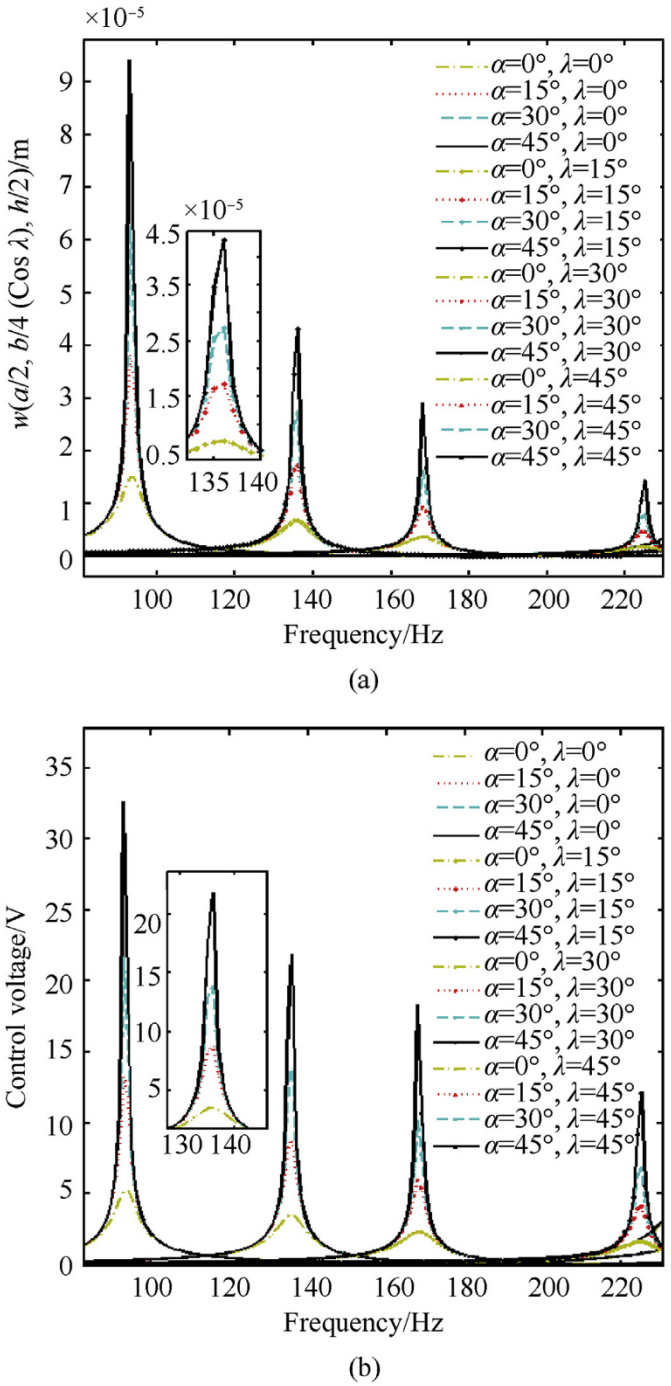

Fig. 7. Effect of piezoelectric fiber orientations of 1–3 PZC on (a) transverse deflection w and (b) control voltage ($r = 1$; B rich bottom; centre patch; $K_d = 600$).

Table 9
Effect of piezoelectric fiber orientation angle on the transverse deflection w ($\times 10^{-5}$ m).

Skew angle	Piezoelectric fiber angle(α)	B rich bottom			F rich bottom		
		$r = 1$	$r = 2$	$r = 5$	$r = 1$	$r = 2$	$r = 5$
$\lambda = 0^o$	0	1.57	1.47	1.38	1.60	1.55	1.42
	15	3.81	3.79	3.42	4.08	3.97	3.52
	30	6.27	6.24	5.39	6.68	6.55	5.55
	45	9.41	9.38	7.47	10.1	11.6	7.73
$\lambda = 15^o$	0	0.68	0.64	0.63	0.74	0.70	0.65
	15	1.72	1.69	1.59	1.82	1.80	1.63
	30	2.72	2.68	2.62	3.1	2.83	2.69
	45	4.36	4.32	4.14	5.87	4.89	4.28
$\lambda = 30^o$	0	0.37	0.35	0.33	0.39	0.37	0.35
	15	0.94	0.90	0.86	1.01	0.93	0.88
	30	1.61	1.57	1.45	1.71	1.52	1.50
	45	2.90	2.86	2.56	3.13	2.66	2.43
$\lambda = 45^o$	0	0.19	0.18	0.17	0.21	0.19	0.18
	15	0.48	0.44	0.43	0.51	0.48	0.45
	30	0.79	0.77	0.75	0.83	0.81	0.78
	45	1.42	1.38	1.36	1.48	1.44	1.42

Table 10
Effect of piezoelectric fiber orientation angle on the required control voltage (in Volts).

Skew angle	Piezoelectric fiber angle(α)	B rich bottom			F rich bottom		
		$r = 1$	$r = 2$	$r = 5$	$r = 1$	$r = 2$	$r = 5$
$\lambda = 0^o$	0	5.28	5.26	5.11	5.808	5.786	5.3655
	15	13.6	13.1	12.50	14.96	14.41	13.125
	30	22.62	21.77	19.72	24.882	23.947	20.706
	45	41.10	32.65	27.34	45.21	35.915	28.707
$\lambda = 15^o$	0	3.52	3.48	3.37	3.872	3.828	3.5385
	15	8.97	8.76	8.46	9.867	9.636	8.883
	30	15.38	14.18	13.94	16.918	15.598	14.637
	45	29.29	22.03	21.39	32.219	24.233	22.4595
$\lambda = 30^o$	0	2.35	2.29	2.21	2.585	2.519	2.3205
	15	5.96	5.76	5.68	6.556	6.336	5.964
	30	10.17	9.66	9.36	11.187	10.626	9.828
	45	18.27	17.03	15.53	20.097	18.733	16.3065
$\lambda = 45^o$	0	1.59	1.58	1.53	1.749	1.738	1.6065
	15	4.07	4.03	3.93	4.477	4.433	4.1265
	30	6.79	6.74	6.73	7.469	7.414	7.0665
	45	12.67	12.34	12.15	13.937	13.574	12.7575

PZC can be noticed if the piezoelectric fibers in it are vertically aligned ($\alpha = 0^o$). Furthermore, the influences of other parameters associated with piezoelectric fiber orientations, on the w and control voltage are illustrated in Tables 9 and 10, respectively. The influence of using different combinations of geometric and material parameters can be observed again. Hence forward, the effect of such increasing phenomenon shall be considered in the design processes.

4. Conclusions

The present article includes an FE procedure to clarify the controlled frequency response of FGSMEE plates coupled with ACLD usage. A simple power-law distribution is assumed to estimate variation of the material properties across the plate thickness. Under the framework of Hamilton's principle, the governing equations of motion are derived incorporating skew transformation and solved through condensation technique. The most important outcomes can be reviewed as follows:

- FGSMEE plates with higher skew angles display increased attenuation capability.
- Controlled linear response can be intensified increasing the power-law index.
- FGSMEE plate with piezoelectric layer rich bottom layer and to piezomagnetic rich top layer yields a lesser vibration amplitude.
- A single centre ACLD patch with vertically reinforced piezoelectric fibers are found to be more efficient for damping when compared to two edge ACLD patches.
- Increasing the control gain results in intensified damping characteristics.

Data availability

The preliminary data essential to replicate these findings cannot be made public at this time as it forms a vital part of an ongoing study.

Declaration of competing interest

The authors declare no impending conflicts of interest with regard to the work, credits, and/or publication of this article.

Acknowledgements

The first author acknowledges the support of Indian Institute of Science, Bangalore through CV Raman Post-Doc Fellowship under Institute of Eminence Scheme.

Appendix-A. Material property matrices

The different material coefficient matrices of FGMEEM appearing in Eq. (1) can be explicitly represented as follows:

$$\left[\overline{C}_b^{fg}(z)\right]=\begin{bmatrix}\overline{C}_{11}^{fg}(z) & \overline{C}_{12}^{fg}(z) & \overline{C}_{13}^{fg}(z) & \overline{C}_{16}^{fg}(z)\\ \overline{C}_{12}^{fg}(z) & \overline{C}_{22}^{fg}(z) & \overline{C}_{23}^{fg}(z) & \overline{C}_{26}^{fg}(z)\\ \overline{C}_{13}^{fg}(z) & \overline{C}_{32}^{fg}(z) & \overline{C}_{33}^{fg}(z) & \overline{C}_{36}^{fg}(z)\\ \overline{C}_{16}^{fg}(z) & \overline{C}_{26}^{fg}(z) & \overline{C}_{36}^{fg}(z) & \overline{C}_{66}^{fg}(z)\end{bmatrix};\quad \left[\overline{C}_s^{fg}(z)\right]=\begin{bmatrix}\overline{C}_{55}^{fg}(z) & \overline{C}_{45}^{fg}(z)\\ \overline{C}_{45}^{fg}(z) & \overline{C}_{66}^{fg}(z)\end{bmatrix};$$

$$\left\{\overline{e}^{fg}\right\}=\begin{Bmatrix}\overline{e}_{31}^{fg}(z)\\ \overline{e}_{32}^{fg}(z)\\ \overline{e}_{33}^{fg}(z)\\ \overline{e}_{36}^{fg}(z)\end{Bmatrix};\quad \left\{\overline{q}^{fg}\right\}=\begin{Bmatrix}\overline{q}_{31}^{fg}(z)\\ \overline{q}_{32}^{fg}(z)\\ \overline{q}_{33}^{fg}(z)\\ \overline{q}_{36}^{fg}(z)\end{Bmatrix} \tag{A-1}$$

Further, the transformed coupling elastic matrices $[\overline{C}_{bs}]$ for the piezoelectric fiber orientation (α) in the *xz*- or *yz*-plane, respectively can be shown as follows:

$$\left[\overline{C}_{bs}^{P}\right]=\begin{bmatrix}\overline{C}_{15}^{P} & \overline{C}_{25}^{P} & \overset{P}{\underset{35}{\overline{C}}} & 0 & 0 & 0 & \overline{C}_{46}^{P}\end{bmatrix}^{\mathrm{T}} \text{ or } \left[\overline{C}_{bs}^{P}\right]$$
$$=\begin{bmatrix}0 & 0 & \overline{C}_{56}^{P} & 0 & \overline{C}_{14}^{P} & \overset{P}{\underset{24}{\overline{C}}} & \overset{P}{\underset{34}{0\overline{C}}}\end{bmatrix}^{\mathrm{T}} \tag{A-2}$$

Also, the elastic stiffness coefficient matrices, piezoelectric coefficient matrices of 1–3 PZC can be given as follows:

$$\left[\overline{C}_b^{P}\right]=\begin{bmatrix}\overline{C}_{11}^{P} & \overline{C}_{12}^{P} & \overline{C}_{13}^{P} & \overline{C}_{16}^{P}\\ \overline{C}_{12}^{P} & \overline{C}_{22}^{P} & \overline{C}_{23}^{P} & \overline{C}_{26}^{P}\\ \overline{C}_{13}^{P} & \overline{C}_{32}^{P} & \overline{C}_{33}^{P} & \overline{C}_{36}^{P}\\ \overline{C}_{16}^{P} & \overline{C}_{26}^{P} & \overline{C}_{36}^{P} & \overline{C}_{66}^{P}\end{bmatrix};\quad \left[\overline{C}_s^{P}\right]=\begin{bmatrix}\overline{C}_{55}^{P} & \overline{C}_{45}^{P}\\ \overline{C}_{45}^{P} & \overline{C}_{66}^{P}\end{bmatrix}$$

$$\left\{\overline{e}_b^{P}\right\}=\begin{Bmatrix}\overline{e}_{31}^{P}\\ \overline{e}_{32}^{P}\\ \overline{e}_{33}^{P}\\ \overline{e}_{36}^{P}\end{Bmatrix};\quad \left\{\overline{e}_s^{P}\right\}=\begin{Bmatrix}\overline{e}_{35}^{P}\\ \overline{e}_{34}^{P}\end{Bmatrix} \tag{A-3}$$

Meanwhile, the stress equation for the viscoelastic layer of ACLD patch can be denoted as follows:

$$\left\{\sigma_s^{V}\right\}=\left[\overline{C}_s^{V}\right]\left\{\varepsilon_s^{V}\right\} \tag{A-4}$$

in which,

$$\left[\overline{C}_s^{V}\right]=\begin{bmatrix}\overline{C}_{55}^{V} & 0 & 0 & \overline{C}_{44}^{V}\end{bmatrix};\ \left\{\varepsilon_s^{V}\right\}=\begin{Bmatrix}\varepsilon_{xz}\\ \varepsilon_{yz}\end{Bmatrix} \tag{A-5}$$

Appendix-B. Strain component and transformation matrices

The strain components appearing in Eqs. (12) and (13) can be illustrated as follows:

$$\{\varepsilon_{bt}\}=\begin{Bmatrix}\partial u_0/\partial x\\ \partial v_0/\partial y\\ 0\\ \partial u_0/\partial y+\partial v_0/\partial x\end{Bmatrix};\ \{\varepsilon_{ts}\}=\begin{Bmatrix}\partial w_0/\partial x\\ \partial w_0/\partial y\end{Bmatrix}$$

$$\{\varepsilon_{rs}\}=\begin{Bmatrix}\theta_x\\ \theta_y\\ \kappa_x\\ \kappa_y\\ \gamma_x\\ \gamma_y\\ \partial\theta_z/\partial x\\ \partial\theta_z/\partial y\\ \partial\kappa_z/\partial x\\ \partial\kappa_z/\partial y\end{Bmatrix};\{\varepsilon_{rb}\}=\begin{Bmatrix}\partial\theta_x/\partial x\\ \partial\theta_y/\partial y\\ \partial\theta_x/\partial y+\partial\theta_y/\partial x\\ \theta_z\\ \kappa_z\\ \partial\kappa_x/\partial x\\ \partial\kappa_y/\partial y\\ \partial\kappa_x/\partial y+\partial\kappa_y/\partial x\\ \partial\gamma_x/\partial x\\ \partial\gamma_y/\partial y\\ \partial\gamma_x/\partial y+\partial\gamma_y/\partial x\end{Bmatrix} \tag{B-1}$$

Also, the different transformation matrices depicted in Eqs. (12) and (13) can be represented as follows:

$$[Z_1]=\begin{bmatrix}z&0&0&0&0&0&0&0&0&0&0\\0&z&0&0&0&0&0&0&0&0&0\\0&0&0&1&2z&0&0&0&0&0&0\\0&0&z&0&0&0&0&0&0&0&0\end{bmatrix}$$

$$[Z_2]=\begin{bmatrix}h/2&0&0&0&0&h_v&0&0&(z-h_v-h/2)&0&0\\0&h/2&0&0&0&0&h_v&0&0&(z-h_v-h/2)&0\\0&0&0&1&2z&0&0&0&0&0&(z-h_v-h/2)\\0&0&h/2&0&0&0&0&h_v&0&0&0\end{bmatrix}$$

$$[Z_3]=\begin{bmatrix}1&0&0&0&0&0&z&0&z^2&0\\0&1&0&0&0&0&0&z&0&z^2\end{bmatrix};\ [Z_4]=\begin{bmatrix}0&0&1&0&0&0&z&0&z^2&0\\0&0&0&1&0&0&0&z&0&z^2\end{bmatrix}$$

$$[Z_5]=\begin{bmatrix}0&0&0&0&1&0&z&0&z^2&0\\0&0&0&0&0&1&0&z&0&z\end{bmatrix} \tag{B-2}$$

The strain-displacement relationship can be explicitly expressed by,

$$[B_{tb}]=\begin{bmatrix}\partial/\partial x&0&0\\0&\partial/\partial y&0\\0&0&0\\\partial/\partial y&\partial/\partial x&0\end{bmatrix};\ [B_{ts}]=\begin{bmatrix}0&0&\partial/\partial x\\0&0&\partial/\partial y\end{bmatrix}$$

$$[B_{rb}]=\begin{bmatrix}\partial/\partial x&0&0&0&0&0&0&0\\0&\partial/\partial y&0&0&0&0&0&0\\\partial/\partial y&\partial/\partial x&0&0&0&0&0&0\\0&0&1&0&0&0&0&0\\0&0&0&1&0&0&0&0\\0&0&0&0&\partial/\partial x&0&0&0\\0&0&0&0&0&\partial/\partial y&0&0\\0&0&0&0&\partial/\partial y&\partial/\partial x&0&0\\0&0&0&0&0&0&\partial/\partial x&0\\0&0&0&0&0&0&0&\partial/\partial y\\0&0&0&0&0&0&\partial/\partial y&\partial/\partial x\end{bmatrix},$$

$$[B_{rs}]=\begin{bmatrix}1&0&0&0&0&0&0&0\\0&1&0&0&0&0&0&0\\0&0&0&0&1&0&0&0\\0&0&0&0&0&1&0&0\\0&0&0&0&0&0&1&0\\0&0&0&0&0&0&0&1\\0&0&\partial/\partial x&0&0&0&0&0\\0&0&\partial/\partial y&0&0&0&0&0\\0&0&0&\partial/\partial x&0&0&0&0\\0&0&0&\partial/\partial y&0&0&0&0\end{bmatrix} \tag{B-3}$$

Appendix C. Stiffness and rigidity matrices

The various elemental stiffness matrices and force vectors appearing in Eq. (30) can be illustrated as follows:

$$[K^e_{tt}] = \left([K^e_{ttc}] + [K^e_{tsv}] + \left[K^e_{tbp}\right] + \left[K^e_{tsp}\right]\right); [K^e_{tr}] = \left([K^e_{trc}] + [K^e_{trsv}] + \left[K^e_{trbp}\right] + \left[K^e_{trsp}\right]\right)$$

$$[K^e_{rr}] = \left([K^e_{rrc}] + [K^e_{rrsv}] + \left[K^e_{rrbp}\right] + \left[K^e_{rrsp}\right]\right); \left\{F^e_{tp}\right\} = \left[\left\{F^e_{tpb}\right\} + \left\{F^e_{tps}\right\}\right]$$

$$\left\{F^e_{rp}\right\} = \left[\left\{F^e_{rpb}\right\} + \left\{F^e_{rps}\right\}\right],\ \{F^e\} = \int_0^{b_e}\int_0^{a_e} [N_t]^{\mathrm{T}}\{f\}\ dxdy\ ,\ [K^e_{ttc}] = [K^e_{tb}] + [K^e_{ts}];\ [K^e_{trc}] = [K^e_{trb}] + [K^e_{trs}];\ [K^e_{rrc}] = [K^e_{rrb}] + [K^e_{rrs}];$$

$$[K^e_{tb}] = \int_0^{a_e}\int_0^{b_e} [B_{tb}]^{\mathrm{T}}[D_{tb}][B_{tb}]\ \mathrm{d}x\mathrm{d}y;\ [K^e_{ts}] = \int_0^{a_e}\int_0^{b_e} [B_{ts}]^{\mathrm{T}}[D_{ts}]\ [B_{ts}]\ \mathrm{d}x\mathrm{d}y$$

$$[K^e_{tsv}] = h_v\int_0^{b_e}\int_0^{a_e} [B_{ts}]^{\mathrm{T}}[B_{ts}]\ \mathrm{d}x\mathrm{d}y,\ \left[K^e_{tbp}\right] = \int_0^{a_e}\int_0^{b_e}\left([B_{tb}]^{\mathrm{T}}\left[D^p_{tb}\right][B_{tb}] + 2[B_{tb}]^{\mathrm{T}}\left[D^p_{tbs}\right][B_{ts}]\right)\mathrm{d}x\mathrm{d}y,$$

$$\left[K^e_{tsp}\right] = \int_0^{a_e}\int_0^{b_e} [B_{ts}]^{\mathrm{T}}[D^p_{ts}][B_{ts}]\ \mathrm{d}x\mathrm{d}y,$$

$$[K^e_{trb}] = \int_0^{a_e}\int_0^{b_e} [B_{tb}]^{\mathrm{T}}[D_{trb}][B_{rb}]\ \mathrm{d}x\mathrm{d}y\ ,\ [K^e_{trs}] = \int_0^{b_e}\int_0^{a_e} [B_{ts}]^{\mathrm{T}}[D_{trs}]\ [B_{rs}]\ \mathrm{d}x\mathrm{d}y;$$

$$[K^e_{trsv}] = \int_0^{b_e}\int_0^{a_e} [B_{ts}]^{\mathrm{T}}[D_{trsv}]\ [B_{rs}]\ \mathrm{d}x\mathrm{d}y,\ \left[K^e_{trbp}\right] = \int_0^{a_e}\int_0^{b_e}\left([B_{tb}]^{\mathrm{T}}\left[D^p_{trb}\right][B_{rb}] + [B_{tb}]^{\mathrm{T}}\left[D^p_{trbs}\right][B_{rs}] + [B_{ts}]^{\mathrm{T}}\left[D^p_{rtbs}\right]^{\mathrm{T}}[B_{rb}]\right)\mathrm{d}x\mathrm{d}y$$

$$\left[K^e_{trsp}\right] = \int_0^{a_e}\int_0^{b_e} [B_{ts}]^{\mathrm{T}}[D^p_{trs}][B_{rs}]\ \mathrm{d}x\mathrm{d}y;$$

$$[K^e_{rrb}] = \int_0^{a_e}\int_0^{b_e} [B_{rb}]^{\mathrm{T}}[D_{rrb}][B_{rb}]\ \mathrm{d}x\mathrm{d}y;$$

$$[K^e_{rrs}] = \int_0^{b_e}\int_0^{a_e} [B_{rs}]^{\mathrm{T}}[D_{rrs}]\ [B_{rs}]\ \mathrm{d}x\mathrm{d}y;$$

$$[K^e_{rrsv}] = \int_0^{b_e}\int_0^{a_e} [B_{rs}]^{\mathrm{T}}[D_{rrsv}]\ [B_{rs}]\ \mathrm{d}x\mathrm{d}y$$

$$[K^e_{rrsv}] = \int_0^{b_e}\int_0^{a_e} [B_{rs}]^{\mathrm{T}}[D_{rrsv}]\ [B_{rs}]\ \mathrm{d}x\mathrm{d}y,$$

$$\left[K^e_{rrbp}\right] = \int_0^{a_e}\int_0^{b_e}\left([B_{rb}]^{\mathrm{T}}\left[D^p_{rrb}\right][B_{rb}] + 2[B_{rb}]^{\mathrm{T}}\left[D^p_{rrbs}\right][B_{rs}]\right)\mathrm{d}x\mathrm{d}y$$

$$\left[K^e_{rrsp}\right] = \int_0^{a_e}\int_0^{b_e} [B_{rs}]^{\mathrm{T}}\left[D^p_{rrs}\right][B_{rs}]\ \mathrm{d}x\mathrm{d}y,\ [K^e_{t\varphi}] = \int_0^{a_e}\int_0^{b_e} [B_{tb}]^{\mathrm{T}}[D_{t\varphi}][N_\varphi]\mathrm{d}x\mathrm{d}y$$

$$[K^e_{r\varphi}] = \int_0^{a_e}\int_0^{b_e} [B_{rb}]^{\mathrm{T}}[D_{r\varphi}][N_\varphi]\mathrm{d}x\mathrm{d}y,\ [K^e_{t\psi}] = \int_0^{a_e}\int_0^{b_e} [B_{tb}]^{\mathrm{T}}[D_{t\psi}][N_\psi]\mathrm{d}x\mathrm{d}y$$

$$[K^e_{r\psi}] = \int_0^{a_e}\int_0^{b_e} [B_{rb}]^{\mathrm{T}}[D_{r\psi}][N_\psi]\mathrm{d}x\mathrm{d}y$$

$$\left\{F^e_{tpb}\right\} = \int_0^{a_e}\int_0^{b_e} [B_{tb}]^{\mathrm{T}}\ \left\{D^b_{tp}\right\}\mathrm{d}x\mathrm{d}y;\ \left\{F^e_{rpb}\right\} = \int_0^{a_e}\int_0^{b_e} [B_{rb}]^{\mathrm{T}}\ \left\{D^b_{rp}\right\}\mathrm{d}x\mathrm{d}y$$

$$[M^e] = \int_0^{b_e}\int_0^{a_e} \overline{m}[N_t]^{\mathrm{T}}[N_t]\ \mathrm{d}x\mathrm{d}y,\ \overline{m} = \sum_{k=1}^{3}\int_{h_k}^{h_{k+1}} \rho_S^k \mathrm{d}z + \int_0^{h_V} \rho_V \mathrm{d}z + \int_0^{h_P} \rho_P \mathrm{d}z \tag{C-1}$$

The various rigidity matrices associated with the elemental stiffness matrices are shown by,

1. Rigidity matrices related to FGSMEE substrate

$$[D_{tb}]=\int_{h_1}^{h_2}\left[\overline{C}_{b}^{fg}(z)\right]\mathrm{d}z,\ [D_{trb}]=\int_{h_1}^{h_2}\left[\overline{C}_{b}^{fg}(z)\right][Z_1]\ \mathrm{d}z,\ [D_{rrb}]$$
$$=\int_{h_1}^{h_2}[Z_1]^{\mathrm{T}}\left[\overline{C}_{b}^{fg}(z)\right][Z_1]\ \mathrm{d}z[D_{ts}]=\int_{h_1}^{h_2}\left[\overline{C}_{s}^{fg}(z)\right]\mathrm{d}z,\ [D_{trs}]$$
$$=\int_{h_1}^{h_2}\left[\overline{C}_{s}^{fg}(z)\right][Z_3]\mathrm{d}z,\ [D_{rrs}]=\int_{h_1}^{h_2}[Z_3]^{\mathrm{T}}\left[\overline{C}_{s}^{fg}(z)\right][Z_3]\ \mathrm{d}z$$

2. Rigidity matrices related to 1–3 PZC layer of ACLD patch

$$\left[D_{tb}^{p}\right]=\int_{h_3}^{h_4}\left[\overline{C}_{b}^{p}\right]\mathrm{d}z,\ \left[D_{trb}^{p}\right]=\int_{h_3}^{h_4}\left[\overline{C}_{b}^{p}\right][Z_2]\mathrm{d}z,\ \left[D_{trb}^{p}\right]=\int_{h_3}^{h_4}\left[\overline{C}_{b}^{p}\right][Z_2]\mathrm{d}z,\ \left[D_{rrb}^{p}\right]=\int_{h_3}^{h_4}[Z_2]^{\mathrm{T}}\left[\overline{C}_{b}^{p}\right][Z_2]\mathrm{d}z,\ [D_{ts}^{p}]=\int_{h_3}^{h_4}[\overline{C}_{s}^{p}]\mathrm{d}z,$$
$$[D_{trs}^{p}]=\int_{h_3}^{h_4}[\overline{C}_{s}^{p}][Z_5]\mathrm{d}z,\ [D_{rrs}^{p}]=\int_{h_3}^{h_4}[Z_2]^{\mathrm{T}}[\overline{C}_{s}^{p}][Z_5]\mathrm{d}z,\ \left[D_{tbs}^{p}\right]=\int_{h_3}^{h_4}\left[\overline{C}_{bs}^{p}\right]\mathrm{d}z,\ \left[D_{rtbs}^{p}\right]=\int_{h_3}^{h_4}[Z_2]^{\mathrm{T}}\left[\overline{C}_{bs}^{p}\right]\mathrm{d}z,\ \left[D_{trbs}^{p}\right]=\int_{h_3}^{h_4}\left[\overline{C}_{bs}^{p}\right][Z_5]\mathrm{d}z,$$
$$\left[D_{trbs}^{p}\right]=\int_{h_3}^{h_4}\left[\overline{C}_{bs}^{p}\right][Z_5]\mathrm{d}z,\ \left[D_{rrbs}^{p}\right]=\int_{h_3}^{h_4}[Z_2]^{\mathrm{T}}\left[\overline{C}_{bs}^{p}\right][Z_5]\mathrm{d}z,\ \left\{D_{tp}^{b}\right\}=\int_{h_3}^{h_4}\frac{1}{h_p}\left\{\overline{e}_{b}^{p}\right\}\mathrm{d}z,\ \left\{D_{rp}^{b}\right\}=\int_{h_3}^{h_4}\frac{1}{h_p}[Z_2]^{\mathrm{T}}\left\{\overline{e}_{b}^{p}\right\}\mathrm{d}z,\ \left\{D_{rp}^{b}\right\}=\int_{h_3}^{h_4}\frac{1}{h_p}[Z_2]^{\mathrm{T}}\left\{\overline{e}_{b}^{p}\right\}\mathrm{d}z,$$
$$\left\{D_{tp}^{s}\right\}=\int_{h_3}^{h_4}\frac{1}{h_p}\{e_{s}^{p}\}\mathrm{d}z,\ \left\{D_{rp}^{s}\right\}=\int_{h_3}^{h_4}\frac{1}{h_p}[Z_5]^{\mathrm{T}}\{\overline{e}_{s}^{p}\}\mathrm{d}z,$$

(C-3)

3. Rigidity matrices related to viscoelastic layer of ACLD patch

$$[D_{tsv}]=\int_{h_2}^{h_3}[\overline{C}_{s}^{v}]\mathrm{d}z,\ [D_{trsv}]=\int_{h_2}^{h_3}[\overline{C}_{s}^{v}][Z_4]\mathrm{d}z,\ [D_{rrsv}]=\int_{h_2}^{h_3}[Z_4]^{\mathrm{T}}[\overline{C}_{s}^{v}][Z_4]\mathrm{d}z$$

(C-4)

Appendix-D. Condensation technique

In this section, the detailed condensation procedure to obtain the natural frequency is depicted.

From Eq. (35d), it can be deduced that

$$\{\psi\}=[K_{\psi\psi}]^{-1}\left[[K_{t\psi}]^{\mathrm{T}}\{d_t\}+[K_{r\psi}]^{\mathrm{T}}\{d_r\}-[K_{\varphi\psi}]^{\mathrm{T}}\{\varphi\}-\{F_{\psi}\}\right]\qquad\text{(D-1)}$$

$$[D_{tb}]=\int_{h_1}^{h_2}\left[\overline{C}_{b}^{fg}(z)\right]\mathrm{d}z,\ [D_{trb}]=\int_{h_1}^{h_2}\left[\overline{C}_{b}^{fg}(z)\right][Z_1]\mathrm{d}z,\ [D_{rrb}]=\int_{h_1}^{h_2}[Z_1]^{\mathrm{T}}\left[\overline{C}_{b}^{fg}(z)\right][Z_1]\mathrm{d}z$$
$$[D_{ts}]=\int_{h_1}^{h_2}\left[\overline{C}_{s}^{fg}(z)\right]\mathrm{d}z,\ [D_{trs}]=\int_{h_1}^{h_2}\left[\overline{C}_{s}^{fg}(z)\right][Z_3]\mathrm{d}z,\ [D_{rrs}]=\int_{h_1}^{h_2}[Z_3]^{\mathrm{T}}\left[\overline{C}_{s}^{fg}(z)\right][Z_3]\mathrm{d}z$$
$$[D_{t\psi}]=\int_{h_1}^{h_2}\left\{\overline{q}_{b}^{fg}\right\}\frac{1}{H}\mathrm{d}z,\ [D_{t\phi}]=\int_{h_1}^{h_2}\{e_{b}^{s}\}\frac{1}{H}\mathrm{d}z,\ [D_{t\phi}]=\int_{h_1}^{h_2}\{e_{b}^{s}\}\frac{1}{H}\mathrm{d}z,$$
$$[D_{r\psi}]=\int_{h_1}^{h_2}[Z_1]^{\mathrm{T}}\{q_{b}^{s}(z)\}\frac{1}{h}\mathrm{d}z,\ [D_{r\phi}]=\int_{h1}^{h_2}[z_1]^{\mathrm{T}}\{e_{b}^{s}(z)\}\frac{1}{H}\mathrm{d}z,\ [D_{\phi\phi}]=\int_{h_1}^{h_2}\frac{\overline{\in}_{33(z)}^{fg}}{H}\mathrm{d}z,\ [D_{\psi\psi}]=\int_{h_1}^{h_2}\frac{\overline{\mu}_{33}^{fg}(z)}{H}\mathrm{d}z$$

(C-2)

By substituting Eq. (D-1) in Eq. (35c), we get,

$$[K_{t\varphi}]^{\mathrm{T}}\{d_t\}+[K_{r\varphi}]^{\mathrm{T}}\{d_r\}-[K_{\varphi\varphi}]\{\varphi\}-[K_{\varphi\psi}]\Big[[K_{\psi\psi}]^{-1}[K_{t\psi}]^{\mathrm{T}}\{d_t\}+[K_{\psi\psi}]^{-1}[K_{r\psi}]^{\mathrm{T}}\{d_r\}-[K_{\psi\psi}]^{-1}[K_{\varphi\psi}]^{\mathrm{T}}\{\varphi\}-[K_{\psi\psi}]^{-1}\{F_\psi\}\Big]=\{F_\varphi\} \tag{D-2}$$

Grouping the terms based of the coefficient of $\{d_t\}$, $\{d_r\}$, $\{\varphi\}$ and $\{\psi\}$, Eq. (D-2) reduces to,

$$[K_1]\{d_t\}+[K_2]\{d_r\}-[K_3]\{\varphi\}=\{F_\varphi\}-[K_{\varphi\psi}][K_{\psi\psi}]^{-1}\{F_\psi\} \tag{D-3}$$

From Eq. (D-3), $\{\varphi\}$ can be obtained as follows:

$$\{\varphi\}=[K_3]^{-1}[K_1]\{d_t\}+[K_3]^{-1}[K_2]\{d_r\}-[K_3]^{-1}\{F_\varphi\}+[K_3]^{-1}[K_{\varphi\psi}][K_{\psi\psi}]^{-1}\{F_\psi\} \tag{D-4}$$

$$\{\varphi\}=[K_4]\{d_t\}+[K_5]\{d_r\}-[K_3]^{-1}\{F_\varphi\}+[K_6]\{F_\psi\} \tag{D-5}$$

Further, substituting (D-1) in Eq. (35b), it be shown that

$$[K_{tr}]^{\mathrm{T}}\{d_t\}+[K_{rr}]\{d_r\}+[K_{r\varphi}]\{\varphi\}+[K_{r\psi}][K_{\psi\psi}]^{-1}\Big[[K_{t\psi}]^{\mathrm{T}}\{d_t\}+[K_{r\psi}]^{\mathrm{T}}\{d_r\}-[K_{\varphi\psi}]^{\mathrm{T}}\{\varphi\}-\{F_\psi\}\Big]=-\{F_{rp}\}V \tag{D-6}$$

Bifurcating and rearranging the terms related to the coefficient of $\{d_t\}$, $\{d_r\}$, $\{\varphi\}$ and $\{\psi\}$, results in

$$[K_7]\{d_t\}+[K_8]\{d_r\}+[K_9]\{\varphi\}=[K_{r\psi}][K_{\psi\psi}]^{-1}\{F_\psi\}-\{F_{rp}\}V \tag{D-7}$$

Now, substituting (D-5) in (D-7) gives,

$$[K_7]\{d_t\}+[K_8]\{d_r\}+[K_9]\Big([K_4]\{d_t\}+[K_5]\{d_r\}-[K_3]^{-1}\{F_\varphi\}+[K_6]\{F_\psi\}\Big)=[K_{r\psi}][K_{\psi\psi}]^{-1}\{F_\psi\}-\{F_{rp}\}V \tag{D-8}$$

which can be simplified to

$$[K_{10}]\{d_t\}+[K_{11}]\{d_r\}=[K_9][K_3]^{-1}\{F_\varphi\}+\Big([K_{r\psi}][K_{\psi\psi}]^{-1}-[K_9][K_6]\Big)\{F_\psi\}-\{F_{rp}\}V \tag{D-9}$$

Using Eq. (D-9), it can be obtained that

$$\{d_r\}=-[K_{11}]^{-1}[K_{10}]\{d_t\}+[K_{11}]^{-1}[K_9][K_3]^{-1}\{F_\varphi\}+[K_{11}]^{-1}[K_{12}]\{F_\psi\}-[K_{11}]^{-1}\{F_{rp}\}V \tag{D10}$$

Following the same procedure of substituting (D-1), (D-5) and (D-10) in Eq. (35a), we get

$$[M]\{\ddot{d}_t\}+[K_{tt}]\{d_t\}+[K_{tr}]\{d_r\}+[K_{t\varphi}]\{\varphi\}+[K_{t\psi}][K_{\psi\psi}]^{-1}\Big[[K_{t\psi}]^{\mathrm{T}}\{d_t\}+[K_{r\psi}]^{\mathrm{T}}\{d_r\}-[K_{\varphi\psi}]^{\mathrm{T}}\{\varphi\}-\{F_\psi\}\Big]=\{F\}-\{F_{tp}\}V \tag{D-11}$$

which can be further simplified upon grouping as follows:

$$[M]\{\ddot{d}_t\}+[K_{13}]\{d_t\}+[K_{14}]\{d_r\}+[K_{15}]\{\varphi\}=\{F\}-\{F_{tp}\}V+[K_{t\psi}][K_{\psi\psi}]^{-1}\{F_\psi\} \tag{D-12}$$

$$[M]\{\ddot{d}_t\}+[K_{16}]\{d_t\}+[K_{17}]\{d_r\}=\{F\}-\{F_{tp}\}V+[K_{15}][K_3]^{-1}\{F_\varphi\}+[K_{18}]\{F_\psi\} \tag{D-13}$$

Finally, Eqs. (35a-d) can be represented as a single equation in the form as follows:

$$[M]\{\ddot{d}_t\}+[K_{16}]\{d_t\}+[K_{17}]\Big(-[K_{11}]^{-1}[K_{10}]\{d_t\}+[K_{11}]^{-1}[K_9][K_3]^{-1}\{F_\varphi\}+[K_{11}]^{-1}[K_{12}]\{F_\psi\}-[K_{11}]^{-1}\{F_{rp}\}V\Big)=\{F\}-\{F_{tp}\}V+[K_{15}][K_3]^{-1}\{F_\varphi\}+[K_{18}]\{F_\psi\} \tag{D-14}$$

$$[M]\{\ddot{d}_t\}+[K]\{d_t\}=\{F\}-\{F_P\}V+[K_{a\varphi}]\{F_\varphi\}+[K_{a\psi}]\{F_\psi\} \tag{D-15}$$

where, the different stiffness matrices contributing to Eq. (D-15) can be encapsulated as follows:

$$[K_1]=[K_{t\varphi}]^{\mathrm{T}}-[K_{\varphi\psi}][K_{\psi\psi}]^{-1}[K_{t\psi}]^{\mathrm{T}};\ [K_2]=[K_{r\varphi}]^{\mathrm{T}}-[K_{\varphi\psi}][K_{\psi\psi}]^{-1}[K_{r\psi}]^{\mathrm{T}};$$
$$[K_3]=[K_{\varphi\varphi}]-[K_{\varphi\psi}][K_{\psi\psi}]^{-1}[K_{\varphi\psi}]^{\mathrm{T}};\ [K_4]=[K_3]^{-1}[K_1];\ [K_5]=[K_3]^{-1}[K_2];\ [K_6]=[K_3]^{-1}[K_{\varphi\psi}][K_{\psi\psi}]^{-1};\ [K_7]=[K_{tr}]^{\mathrm{T}}+[K_{r\psi}][K_{\psi\psi}]^{-1}[K_{t\psi}]^{\mathrm{T}}$$
$$[K_8]=[K_{rr}]+[K_{r\psi}][K_{\psi\psi}]^{-1}[K_{r\psi}]^{\mathrm{T}};\ [K_9]=[K_{r\varphi}]-[K_{r\psi}][K_{\psi\psi}]^{-1}[K_{\varphi\psi}]^{\mathrm{T}};\ [K_{10}]=[K_7]+[K_9][K_4];\ [K_{11}]=[K_8]+[K_9][K_5]$$
$$[K_{12}]=[K_{r\psi}][K_{\psi\psi}]^{-1}-[K_9][K_6];\ [K_{13}]=[K_{tt}]+[K_{t\psi}][K_{\psi\psi}]^{-1}[K_{t\psi}]^{\mathrm{T}};$$
$$[K_{14}]=[K_{tr}]+[K_{t\psi}][K_{\psi\psi}]^{-1}[K_{r\psi}]^{\mathrm{T}};\ [K_{15}]=[K_{t\varphi}]-[K_{t\psi}][K_{\psi\psi}]^{-1}[K_{\varphi\psi}]^{\mathrm{T}}\ [K_{16}]=[K_{13}]+[K_{15}][K_4];\ [K_{17}]=[K_{14}]+[K_{15}][K_5];$$
$$[K_{18}]=[K_{t\psi}][K_{\psi\psi}]^{-1}-[K_{15}][K_6][K]=[K_{16}]-[K_{17}][K_{11}]^{-1}[K_{10}];\ [K_{a\varphi}]=[K_{15}][K_3]^{-1}-[K_{17}][K_{11}]^{-1}[K_9][K_3]^{-1}$$
$$[K_{a\psi}]=[K_{18}]-[K_{17}][K_{11}]^{-1}[K_{12}];\ \{F_P\}=[K_{17}][K_{11}]^{-1}\{F_{rp}\}-\{F_{tp}\} \tag{D-16}$$

References

[1] Rabczuk T, Ren H, Zhuang X. A nonlocal operator method for partial differential equations with application to electromagnetic waveguide problem. Comput Mater Continua (CMC) 2019;59(1):31–55.
[2] Ren H, Zhuang X, Rabczuk T. A nonlocal operator method for solving partial differential equations. Comput Methods Appl Mech Eng 2020;358:112621. 2020.
[3] Vinyas M, Kattimani SC. Investigation of the effect of $BaTiO_3/CoFe_2O_4$ particle arrangement on the static response of magneto-electro-thermo-elastic plates. Compos Struct 2018a;185:51–64.
[4] Vinyas M, Kattimani SC, Loja MAR, Vishwas M. Effect of BaTiO3/CoFe2O4 micro-topological textures on the coupled static behaviour of magneto-electro-thermo-elastic beams in different thermal environment. Mater Res Express 2018a;5:125702.
[5] Hamdia KM, Ghasemi H, Zhuang X, Alajlan N, Rabczuk T. Sensitivity and uncertainty analysis for flexoelectric nanostructures. Comput Methods Appl Mech Eng 2018;337:95–109.
[6] Pan E. Exact solution for simply supported and multilayered magneto-electro-elastic plates. J Appl Mech 2001;68:608–18.
[7] Pan E, Heyliger PR. Free vibrations of simply supported and multilayered magneto-electro-elastic plates. J Sound Vib 2002;252(3):429–42.
[8] Lage RG, Soares CM, Soares CA, Reddy JN. Layerwise partial mixed finite element analysis of magneto-electro-elastic plates. Comput Struct 2004;82(17):1293–301.
[9] Moita JMS, Soares CMM, Soares CAM. Analyses of magneto-electro-elastic plates using a higher order finite element model. Compos Struct 2009;91(4):421–6.
[10] Ramirez F, Heyliger PR, Pan E. Free vibration response of two-dimensional magneto-electro-elastic laminated plates. J Sound Vib 2006;292(3):626–44.
[11] Annigeri AR, Ganesan N, Swarnamani S. Free vibration behavior of multiphase and layered magneto-electro-elastic beam. J Sound Vib 2007;299(1):44–63.
[12] Vinyas M, Kattimani SC. Finite element evaluation of free vibration characteristics of magneto-electro-elastic plates in hygrothermal environment using higher order shear deformation theory. Compos Struct 2018b;202:1339–52.
[13] Vinyas M, Piyush JS, Kattimani SC. Influence of coupled fields on free vibration and static behavior of functionally graded magneto-electro-thermo-elastic plate. J Intell Mater Syst Struct 2018b;29(7):1430–55.
[14] Vinyas M, Sunny KK, Harursampath D, Trung NT, Loja MAR. Influence of interphase on the multi-physics coupled frequency of three phase smart magneto-electro-elastic composite plates. Compos Struct 2019;226:111254.
[15] Vinyas M, Nischith G, Loja MAR, Ebrahimi F, Duc ND. Numerical analysis of the vibration response of skew magneto-electro-elastic plates based on the higher-order shear deformation theory. Compos Struct 2019;214:132–42.
[16] Vinyas M. A higher order free vibration analysis of carbon nanotube-reinforced magneto-electro-elastic plates using finite element methods. Compos Part B 2019;158:286–301.
[17] Vinyas M, Sandeep AS, Trung NT, Ebrahimi F, Duc ND. A finite element based assessment of free vibration behaviour of circular and annular magneto-electro-elastic plates using higher order shear deformation theory. J Intell Mater Syst Struct 2019;30(6):2478–501.
[18] Vinyas M, Kattimani SC, Harursampath D, Nguyen Thoi-T. Coupled evaluation of the free vibration characteristics of magneto-electro-elastic skew plates in hygrothermal environment. Smart Struct Syst 2019;24(2):267–92.
[19] Sladek J, Sladek V, Krahulec S, Pan E. The MLPG analyses of large deflections of magnetoelectroelastic plates. Eng Anal Bound Elem 2013;37(4):673–82.
[20] Wang J, Chen L, Fang S. State vector approach to analysis of multilayered magneto-electro-elastic plates. Int J Solids Struct 2003;40(7):1669–80.
[21] Chen WQ, Lee KY. Alternative state space formulations for magnetoelectric thermoelasticity with transverse isotropy and the application to bending analysis of nonhomogeneous plates. Int J Solids Struct 2003;40(21):5689–705.
[22] Chen WQ, Lee KY, Ding HJ. On free vibration of non-homogeneous transversely isotropic magneto-electro-elastic plates. J Sound Vib 2005;279(1–2):237–51.
[23] Xin L, Hu Z. Free vibration of simply supported and multilayered magneto-electro-elastic plates. Compos Struct 2015;121:344–50.
[24] Chen JY, Heyliger PR, Pan E. Free vibration of three-dimensional multilayered magneto-electro-elastic plates under combined clamped/free boundary conditions. J Sound Vib 2014;333(17):4017–29.
[25] Alaimo A, Milazzo A, Orlando C. A four-node MITC finite element for magneto-electro-elastic multilayered plates. Comput Struct 2013;129:120–33.
[26] Benedetti I, Milazzo A. Advanced models for smart multilayered plates based on reissner mixed variational theorem. Compos B Eng 2017;119:215–29.
[27] Milazzo A. A one-dimensional model for dynamic analysis of generally layered magneto-electro-elastic beams. J Sound Vib 2013;332(2):465–83.
[28] Milazzo A. Layer-wise and equivalent single layer models for smart multilayered plates. Compos B Eng 2014a;67:62–75.
[29] Milazzo A. Refined equivalent single layer formulations and finite elements for smart laminates free vibrations. Compos B Eng 2014b;61:238–53.
[30] Guo H, Zhuang X, Rabczuk T. A deep collocation method for the bending analysis of Kirchhoff plate. Comput Mater Continua (CMC) 2019;59(2):433–56.
[31] Anitescu C, Atroshchenko E, Alajlan N, Rabczuk T. Artificial neural network methods for the solution of second order boundary value problems. Comput Mater Continua (CMC) 2019;59(1):345–59.
[32] Pan E, Han F. Exact solution for functionally graded and layered magneto-electro-elastic plates. Int J Eng Sci 2005;43:321–39.
[33] Huang DJ, Ding HJ, Chen WQ. Analytical solution for functionally graded magneto-electro-elastic plane beams. Int J Eng Sci 2007;45(2):467–85.
[34] Bhangale RK, Ganesan N. Free vibration of simply supported functionally graded and layered magneto-electro-elastic plates by finite element method. J Sound Vib 2006;294(4):1016–38.
[35] Wu CP, Tsai YH. Static behavior of functionally graded magneto-electro-elastic shells under electric displacement and magnetic flux. Int J Eng Sci 2007;45:744–69.
[36] Li XY, Ding HJ, Chen WQ. Three-dimensional analytical solution for functionally graded magneto-electro-elastic circular plates subjected to uniform load. Compos Struct 2008;83:381–90.
[37] Sladek J, Sladek V, Krahulec S, Chen CS, Young DL. Analyses of circular magnetoelectroelastic plates with functionally graded material properties. Mecha Adv Mater Struct 2015;22:479–89.
[38] Kiran MC, Kattimani SC, Vinyas M. Porosity influence on structural behaviour of skew functionally graded magneto-electro-elastic plate. Compos Struct 2018;191:36–77.
[39] Vinyas M, Kattimani SC. Static studies of stepped functionally graded magneto-electro-elastic beam subjected to different thermal loads. Compos Struct 2017a;163:216–37.
[40] Vinyas M, Kattimani SC. Static analysis of stepped functionally graded magneto-electro-elastic plates in thermal environment: a finite element study. Compos Struct 2017b;178:63–85.
[41] Vinyas M, Kattimani SC. A Finite element based assessment of static behavior of multiphase magneto-electro-elastic beams under different thermal loading. Struct Eng Mech 2017c;62(5):519–35.
[42] Vinyas M, Kattimani SC. Hygrothermal coupling analysis of magneto-electroelastic beams using finite element methods. J Therm Stress 2017d;41(8):1063–79.
[43] Vinyas M, Kattimani SC. Hygrothermal analysis of magneto-electro-elastic plate using 3D finite element analysis. Compos Struct 2017e;180:617–37.
[44] Newnham RE, Bowen LJ, Klicker KA, Cross LE. Composite piezoelectric transducers. Mater Des 1980;2:93–106.
[45] Ray MC, Pradhan AK. On the use of vertically reinforced 1-3 piezoelectric composites for hybrid damping of laminated composite plates. Mech Adv Mater Struct 2007;14(4):245–61.
[46] Ray MC, Pradhan AK. Performance of vertically reinforced 1–3 piezoelectric composites for active damping of smart structures. Smart Mater Struct 2006;15:631–41.
[47] Panda S, Ray MC. Nonlinear analysis of smart functionally graded plates integrated with a layer of piezoelectric fiber reinforced composite. Smart Mater Struct 2006;15:1595–604.
[48] Panda S, Ray MC. Active control of geometrically nonlinear vibrations of functionally graded laminated composite plates using piezoelectric fiber reinforced composites. J Sound Vib 2009;325:186–205.
[49] Kumar RS, Ray MC. Smart damping of geometrically nonlinear vibrations of functionally graded sandwich plates using 1–3 piezoelectric composites. Mech Adv Mater Struct 2016;23:652–69.
[50] Ray MC, Mallik N. Performance of smart damping treatment using piezoelectric fiber reinforced composites. AIAA J 2005;43:184–93.
[51] Shivakumar J, Ray MC. Nonlinear analysis of smart cross-ply composite plates integrated with a distributed piezoelectric fiber reinforced composite actuator. Mech Adv Mater Struct 2008;15:40–52.
[52] Ray MC, Shivakumar J. Active constrained layer damping of geometrically nonlinear transient vibrations of composite plates using piezoelectric fiber-reinforced composite. Thin-Walled Struct 2009;47:178–89.
[53] Kumar RS, Ray MC. Active constrained layer damping of smart laminated composite sandwich plates using 1–3 piezoelectric composites. Int J Mech Mater Des 2012a;8:197–218.
[54] Kumar RS, Ray MC. Active constrained layer damping of geometrically nonlinear vibrations of smart laminated composite sandwich plates using 1–3 piezoelectric composites. Int J Mech Mater Des 2012b;8:359–80.
[55] Kanasogi RM, Ray MC. Active constrained layer damping of smart skew laminated composite plates using 1–3 piezoelectric composites. J Compos 2013:17. Article ID 824163.
[56] Kattimani SC, Ray MC. Smart damping of geometrically nonlinear vibrations of magneto-electro-elastic plates. Compos Struct 2014;114:51–63.
[57] Kattimani SC, Ray MC. Control of geometrically nonlinear vibrations of functionally graded magneto-electro-elastic plates. Int J Mech Sci 2015;99:154–67.
[58] Kattimani SC, Ray MC. Vibration control of multiferroic fibrous composite plates using active constrained layer damping. Mech Syst Signal Process 2018;106:334–54.
[59] Vinyas M. Vibration control of skew magneto-electro-elastic plates using active constrained layer damping. Compos Struct 2019;208:600–17.
[60] Vinyas M, Kattimani SC. Finite element simulation of controlled frequency response of skewed multiphase magneto-electro-elastic plates. J Intell Mater Syst Struct 2019;30(12):1757–71.
[61] Baz A, Ro J. Optimum design and control of active constrained layer damping. J Vib Acoust 1995;117:135–44.